The gas content variation in the mass-metallicity relation

Babs Beemster and Sascha Zeegers
Supervisor: Dr. Jarle Brinchmann
Leiden Observatory

July 1st 2009

Abstract

For the first time, we derive a clear relation for the gas content variation in the mass-metallicity relation (MZR). First we determine the minimum amount of optical emission lines needed to get good estimates for the gas surface mass density ($\mu_{\rm gas}$) by using a small sample of star-forming galaxies spanning a range in mass and signal to noise. We do a qualitative examination by looking at the trend between log(Hα/Hβ) and $\mu_{\rm gas}$ and determine when the results are no longer physically meaningful. This results in the following minimum required set of optical emission lines: Hβ , [OIII]λ5007 , Hα , [NII]λ6584. We test our gas estimates by comparing them to estimates from CO emission. We find a large discrepancy, for which we cannot find an explanation. We use a sample of $\sim 10^5$ galaxies with spectra from the seventh data release (DR7) of the Sloan Digital Sky Survey and use a pre-existing data set of gas and oxygen abundance estimates that satisfies our requirements. We derive the MZR and investigate the spread. We also investigate the scatter in the effective yield, concluding that galaxies do not evolve as closed box models. To investigate this further, we examine the gas fractions and how it varies in the MZR-plane. We show, that for fixed total mass, galaxies with lower metallicities than the galaxies on the MZR have larger gas fractions than galaxies on the MZR. Also, galaxies with higher metallicities than galaxies on the MZR, have smaller gas fractions than galaxies on the MZR. This is a strong argument for metal-loss by inflow of metal-poor gas. Lower gas fractions are likely to be caused by galactic winds. **Key words**: galaxies: abundances - galaxies: evolution - galaxies: fundamental parameters

1 Introduction

In astronomy, a subject of great interest is the gas content of galaxies. If we want to know how galaxies evolve, we need to understand how gas content and star formation change with time. The standard model of galaxy formation posits that galaxies form when gas cools, condenses and forms stars at the centres of dark matter halos. The massive stars will ionize the gas and enrich it with ejecta of their nucleosynthetic products. It is therefore most important to develop methods to derive gas content, that can be applied to many galaxies.

There are already a few methods to estimate the gas content of galaxies. Tremonti et al. (2004) invert the Schmidt starformation law of Kennicutt (1998) to calculate gas surface densities. A disadvantage of using this law is that it is not certain that this law can be applied at high redshift ($z > 2$). Leroy et al. (2008) used a method that combines the atomic HI gas surface mass densities (derived from 21 cm line integrated intensity maps obtained by Walter et al. (2008)) and molecular H_2 gas surface mass densities using CO emission lines to map the gas surface mass densities for nearby galaxies. Gas content can also be derived by calculating the gas-to-stellar mass ratio based on the analysis of Kannappan et al. (2004) using radio observations of atomic HI gas (like Zhang et al. (2009) did). Both the CO emission lines and the 21 cm line (used to map HI) are measured in the radio part of the spectrum. The difficulty here is that it cannot be used at high redshift. The CO emission line and the 21 cm line can only be observed for nearby galaxies. Also these methods can't be applied to very large samples. We use data of a large sample of galaxies from the Sloan Digital Sky Survey. The radio observations have low spatial resolution and give gas content estimates for the entire galaxy, while the SDSS spectra come from fibres with 3" diameter and thus for the nearby galaxies with radio data they probe only a few percent of the entire galaxy. Thus the two are badly mismatched and one needs complex aperture corrections to compare these two.

With these gas estimates one can derive the gas content variation in the mass-metallicity relation. The relation between mass and metallicity was first explored by Lequeux et al. (1979) and later by Garnett (2002). At that time, obtaining good mass estimates was very difficult, so luminosity was adopted as a measure for mass. However, since the optical luminosity depends strongly on a galaxy's star formation history and metallicity, the stellar mass of a galaxy cannot be directly inferred from that. The first relationship between stellar mass and metallicity was derived by Tremonti et al. (2004). They showed that there is a tight correlation between stellar mass and metallicity. The existence of this tight correlation shows the important role that the mass of a galaxy plays in its chemical evolution. Tremonti et al. also tried to derive the gas content variation in the mass-metallicity relation. They find that galaxies suffer from metal loss due to galactic winds and that galaxies do not evolve as closed box models. Zhang et al. (2009) found that gas-poor galaxies are more metal rich at fixed mass.

In this paper we present a simple method to estimate gas column densities. We make use of the models of Charlot and Longhetti (2001). With these estimates we then derive the gas content variation in the mass-metallicity relation. We will discuss the data in section 2. In section 3 we will explain the model we used to derive the gas content. In section 4 we will test our gas surface mass densities by comparing them to those derived using CO emission by Leroy et al. (2008). In section 5 we will derive what minimum set of emission lines is needed for our study. The gas content variation in the mass-metallicity will be derived in section 6. Will conclude in section 7 with a summary and in section 8 we give a discussion of our results.

2 Data

2.1 The SDSS Data

We use the galaxies of the Sloan Digital Sky Survey (SDSS) Data Release 7 (DR7) database as our parent sample. The SDSS survey goal was to map one quarter of the sky, the project finished in 2008. The SDSS project was done by using a 2.5 meter telescope at Apache Point Observatory, with a special drift scan camera mounted onto it. The imaging data are photometrically calibrated and are used to select objects for fibre spectroscopy. This is done by assigning spectroscopic fibres to the objects on the sky, according to the criteria described in Strauss et al. (2002). Fibres 3"in diameter are manually plugged into drilled aluminium plates mounted at the focal plane of the telescope. The wavelength range is 3800-9200Å. The DR7 is the seventh major data release and provides images, imaging catalogues, spectra, and redshifts. The catalogue derived from the images includes more than 350 million celestial objects, and spectra of 930,000 galaxies, 120,000 quasars, and 460,000 stars. The redshift distribution of the whole galaxy sample extends from 0.005 to 0.33. In spite of the general high quality of the SDSS spectra, the spectrophotometric calibration and the small size of the fiber aperture relative to the target galaxies give some reason for concern. The spectra are frequently acquired under non-photometric conditions, but the survey has been able to obtain a remarkable level of spectrophotometric precision by observing multiple standard stars simultaneously with the target objects. A more serious problem is the size of the fiber aperture. At a median redshift of the DR7 galaxy sample (z≈0.1) the target galaxies subtend several arcseconds on the sky. The fraction of galaxy light falling in the 3" fibre aperture is typically about $\frac{1}{3}$, with variations in redshift and morphological type causing the fraction to range from 0.05 to 0.6.[1] We will discuss the impact of this variation in section 5. We make use of the data provided by J. Brinchmann[2] for star formation rate (SFR) and gas surface mass density estimates. We also use stellar mass estimates from Kauffmann et al. (2003).

2.2 Sample selection

The very large database enables us to make several selection criteria without losing too much data. The first selections we make are selections for the whole SDSS sample.

The first restriction on our sample is a redshift cut of z>0.01 which we make for the whole SDSS DR7 sample. We make this redshift cut because for nearby galaxies, the spectrograph may split a galaxy into several components at low redshift. This may cause the values for the mass to be underestimated. Another reason is that too much light of the galaxy will fall outside the fibre aperture for galaxies at low redshift (see above)[3].

We also note that the emission line [OII]λ3727 cannot be observed at a redshift lower than 0.02, because then [OII]λ3727 falls outside the wavelength range of the SDSS spectrograph, this will affect less than 4% of our sample, but it has a negligible effect on our estimates. We will explain this in further detail in section 4. We use only the spectra of the star-forming galaxies, because our methods cannot be applied to active galactic nuclei (AGN). The models assume that only stars ionize the gas in the galaxies. In the case of AGN the broad and strong emission lines are caused by an active nucleus that ionizes the gas, so the models are unable to account for the source of the emission lines. Separating the AGN from the star-forming galaxies is done by using the standard Baldwin, Phillips & Terlevich (1981, hereafter BPT) classification diagram (see Kaufmann et al. 2003 and Brinchmann et al. 2004 for more details), shown in figure 1.

We now select three samples. The first is a small sample of 100 galaxies. This is a sufficiently small sample to study in detail, but not large enough to study statistics. The second is a separate sample to test the models for some objects in the SDSS database that have extreme spectra and the third is a large sample of 123488 star-forming galaxies that satisfy the criteria

[1] www.sdss.org/dr7
[2] Some of these data are available at http://www.mpa-garching.mpg.de/SDSS/
[3] www.sdss.org/dr7

above.

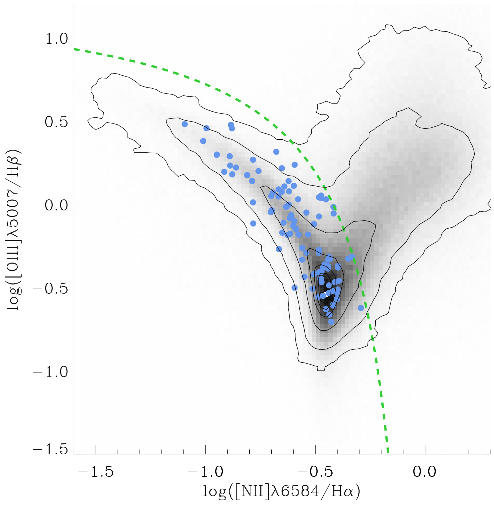

Figure 1: We show Sample I represented by the blue dots in the [OIII]λ5007 /Hβ versus [NII]λ6584 /Hα plane, also referred to as BPT plane. The grey-scale used here, is a two dimensional histogram of the SDSS DR7 galaxies. Bins containing the largest number of galaxies are black, whereas bins containing a low number of galaxies are light grey. The green line separates the galaxies classified as star-forming from the AGN, i.e. objects above this line are AGN and objects below this line are star-forming galaxies. As you can see, Sample I is well-distributed over the the region representing star-forming galaxies in the BPT plane

Sample I

First we selected a sample of star-forming galaxies spanning a range in mass and signal to noise ratio (SNR). The galaxies in the SDSS are not uniformly distributed in mass and SNR, so if we just select 100 galaxies from the data, our sample wil not have a random distribution. To solve this problem we created 10 bins with ranges in SNR and mass. The mass range is: 10^9 $M_\odot$ to 10^{11} $M_\odot$ (divided in equal bins) and the SNR range is: $5 <$ SNR < 10 and SNR $>$20 (so 2 bins). This gives us the $2 \times 5 = 10$ bins. From each bin we randomly chose 10 galaxies. We calculated the signal to noise ratio by dividing the signal of the [NII]λ6584 by the noise of this line. The values are given in the SDSS database. We use [NII]λ6584 because if the SNR in [NII]λ6584 is high enough, it will probably be high enough for all lines. In figure 2 we plot the 10 bins with the randomly chosen galaxies. With the emission lines of the spectra of these galaxies we calculated the gas surface mass densities. We have tested these values as we will show below.

Test sample: Pea objects

The second time we use the models, we apply them to an existing sample of galaxies, namely Pea galaxies or Peas. They are discussed in more detail in section 3.4. It is a relatively small sample of 40 galaxies. It is a subset of a sample of galaxies selected primarily to have a very large equivalent width (EW) in [OIII]λ5007 EW([OIII]λ5007) >500Å for a study of emission line variability in SDSS DR7 galaxies. The sample will be published in York et al (in prep).

Sample II

We have determined what minimum requirements exist for estimating the gas content (see section 4). We select a sample of 123,488 star-forming galaxies, with SNR > 5 that satisfy these criteria and the overall criteria mentioned above. Now we can use a pre-existing data set for the gas estimates (Brinchmann et al. in prep.), the stellar mass densities and the stellar masses (Kauffmann et al. 2003).

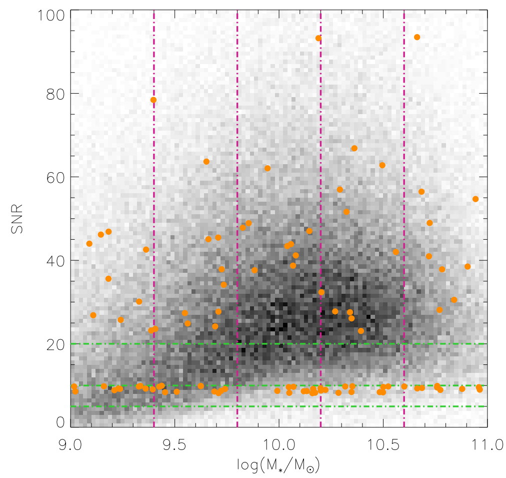

Figure 2: Here we show the 10 bins for different SNR and mass ranges with the randomly chosen galaxies in the M_*-SNR plane. The dashed lines indicate the boundaries of the bins. We chose the galaxies as indicated, randomly drawing 10 per $M_{\rm tot}$-SNR bin. The grey-scale indicates a two-dimensional histogram of the star-forming galaxies in the SDSS DR7.

3 Models

3.1 Explanation of models

We use the model of Charlot and Longhetti (2001; hereafter CL01) to derive estimates of gas surface mass densities ($\mu_{\rm gas}$) for star-forming galaxies. CL01 is based on three different models, i.e. Cloudy (Ferland 1996), BC02 (Bruzual & Charlot 1993) and CF00 (Charlot & Fall 2000).

CL01 uses the stellar population synthesis code BC02 to model a stellar radiation field for a stellar population of a given age. Then it uses CF00, which is discussed below, to determine how the light is attenuated by the interstellar medium (ISM). The obtained spectrum is then run through the photoionization code Cloudy. Cloudy determines how the ultraviolet part of the spectrum is distributed into emission lines. After that, CL01 runs the spectrum with emission lines through CF00 again, which returns the modelled observed fluxes.

BC02 returns the luminosity per unit wavelength per unit mass produced by a stellar population of age t', $S_\lambda(t')$. From Cloudy, CL01 calculates a transmission function $T_\lambda^+(t')$ for the ionized gas (for further details we refer the reader to Charlot & Longhetti 2001). From CF00, it calculates the transmission function $T_\lambda^{\rm ISM}(t')$ for the neutral ISM (birth clouds plus ambient ISM):

$$T_\lambda^{\rm ISM}(t') = \exp[-\tau_\lambda], \quad (1)$$

where τ_λ is the effective optical depth per unit wavelength.

With the above parameters, CL01 creates a model spectrum, calculating the luminosity per unit wavelength $L_\lambda(t)$ emerging at time t from a star-forming galaxy:

$$L_\lambda(t) = \int_0^t {\rm d}t' \psi(t-t') S_\lambda(t') T_\lambda^+(t') T_\lambda^{\rm ISM}(t'), \quad (2)$$

where $\psi(t-t')$ is the star formation rate at time $t-t'$ and t is the stellar age.

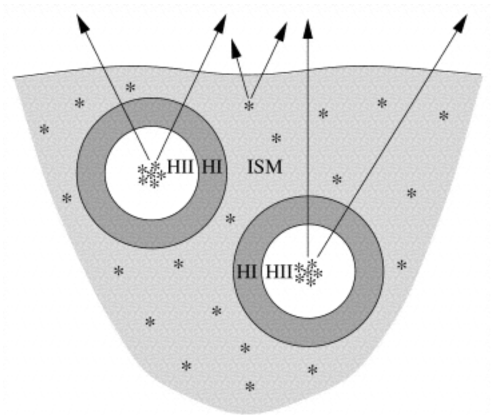

Figure 3: Schematic representation of stellar birth clouds and ambient ISM. Stars are born in birth clouds, which have a finite lifetime. Stars that live longer than their birth clouds, move to the ambient ISM. Rays leaving in different directions are also shown (Charlot & Fall 2000).

CF00 is a simple model for the absorption of starlight by dust in galaxies. It adopts the following view (also see Figure 3): Stars are born in birth clouds, which have a finite lifetime of typically 10^7 years and are assumed to be spherical. When they are born, stars start to ionize the gas around them, creating HII regions. Around these ionized regions is a recombination zone, the HI envelope. Stars that live longer than their birth clouds, will migrate away from them to the ambient interstellar medium (ISM). Line photons produced by young stars residing in their birth clouds, propagate trough the HI envelopes and the ambient ISM, whereas photons emitted by older stars, i.e. stars that have outlived their birth clouds, will only travel through the ambient ISM. The HI and HII regions of the birth clouds may contain dust and the ISM has dust distributed in a smooth or patchy way. Therefore light from young stars will be attenuated by both the birth clouds and the ambient ISM before it escapes from a galaxy, whereas light from old stars will only be attenuated by the ambient ISM. Thus the total flux per wavelength unit that is observed is:

$$F_{\rm tot}^{\rm obs}(\lambda, t) = F_{\rm young}(\lambda, t) e^{-(\tau_{\rm V}^{\rm BC} + \tau_{\rm V}^{\rm ISM})} + F_{\rm old}(\lambda, t) e^{-\tau_{\rm V}^{\rm ISM}}, \quad (3)$$

where $F_{\rm tot}^{\rm obs}(\lambda, t)$ is the total observed flux, $F_{\rm young}(\lambda, t)$ the flux from young stars, $F_{\rm old}(\lambda, t)$ the flux from old stars, $\tau_{\rm V}^{\rm BC}$ the dust attenuation from birth clouds and $\tau_{\rm V}^{\rm ISM}$ the dust attenuation from the ambient ISM.

The derivation of $\mu_{\rm gas}$ here follows closely that of Brinchmann et al. (in prep.). The total effective dust attenuation is the sum of the separate attenuations, i.e.

$$\tau_{\rm V} = \tau_{\rm V}^{\rm BC} + \tau_{\rm V}^{\rm ISM}. \quad (4)$$

$\tau_{\rm V}^{\rm ISM}$ is typically only about $\frac{1}{3}$ of the total dust attenuation (Charlot & Fall 2000), although it turns out that the actual value does not matter. We use the following definitions to derive the surface mass density of gas contributed by the birth clouds:

$$\xi = \mu_{\rm d}/\mu_{\rm Z} \quad (5)$$

and

$$Z = \mu_{\rm Z}/\mu_{\rm gas}, \quad (6)$$

where ξ is the dust-to-metal ratio of the ionized gas, Z the metallicity, $\mu_{\rm d}$ is the surface mass density of dust and $\mu_{\rm Z}$ that of metals. This gives us:

$$\mu_{\rm gas}^{\rm BC} = \tau_{\rm V}^{\rm BC} m_{\rm d}/(\sigma_{\rm d} \xi Z), \quad (7)$$

where $m_{\rm d}$ is the mass of the dust grain and $\sigma_{\rm d}$ its optical cross-section.

CF00 presented that a Poisson distribution of discrete clouds best fitted their data. Then the attenuation in the diffuse ISM is simply:

$$\tau_{\rm V}^{\rm ISM} = \overline{n}[1 - e^{-\tau_{\rm V}^{\rm c}}], \quad (8)$$

where $\tau_{\rm V}^{\rm c}$ is the attenuation per cloud and $\overline{n}$ is the mean number of clouds encountered along different lines of sight. For starburst galaxies, which Charlot & Fall analysed, the best-fit value of $\tau_{\rm V}^{\rm c}$ is 0.3 for optically thin clouds. Furthermore, we assume forward scattering of light. This means that the photons are scattered in such a way that they end up travelling in roughly the same direction as they initially started. This assumption seems to be well supported by both models and observations of interstellar dust in the Milky Way. Now the mean surface mass density of gas along different lines of sight in the ISM is simply:

$$\mu_{\rm gas}^{\rm ISM} = \overline{n} \mu_{\rm gas}^{\rm c}, \quad (9)$$

where $\mu_{\rm gas}^{\rm c}$ is the surface mass density of individual clouds. Strictly speaking, we have adopted a Poisson distribution of identical, face-on screens, rather than one of spherical clouds, but we ignore this subtlety here

Parameter	Description	Range
Z	The metallicity	-1< log(Z/Z$_\odot$) < 0.6 in 24 steps
U	The ionization parameter	-4 < log U <-2 in 33 steps
τ_V	The dust attenuation	0.01 < τ_V < 4.0 in 24 steps
ξ	The dust-to-metal ratio	0.1 < ξ < 0.5 in 9 steps

Table 1: The parameters varied to calculate the model grid. Indicated is the range and the number of steps used to vary.

(for further reference, see Charlot & Fall 2000). From equations 8 and 9 we get:

$$\mu_{\rm gas}^{\rm ISM} = \frac{\tau_V^{\rm ISM}\mu_{\rm gas}^{\rm c}}{1-e^{-\tau_V^{\rm c}}}. \quad (10)$$

Now the surface mass density of an individual cloud can be defined similar to equation 7:

$$\mu_{\rm gas}^{\rm c} = \tau_V^{\rm c} m_{\rm d}/(\sigma_{\rm d}\xi Z). \quad (11)$$

Since $\tau_V^{\rm c} = 0.3$, the surface mass density for gas in the diffuse ISM then becomes:

$$\mu_{\rm gas}^{\rm ISM} = \frac{\tau_V^{\rm c}\tau_V^{\rm ISM} m_{\rm d}}{\sigma_{\rm d}\xi Z[1-e^{-\tau_V^{\rm c}}]} \quad (12)$$

$$= [1+\frac{1}{2}\tau_V^{\rm c} + O((\tau_V^{\rm c})^2)]\frac{\tau_V^{\rm ISM} m_{\rm d}}{\sigma_{\rm d}\xi Z} \quad (13)$$

$$\approx \frac{\tau_V^{\rm ISM} m_{\rm d}}{\sigma_{\rm d}\xi Z}. \quad (14)$$

Note that this approximation will break down for more optically thick clouds. Combining the previously described assumptions, we can write

$$\mu_{\rm gas} = \mu_{\rm gas}^{\rm BC} + \mu_{\rm gas}^{\rm ISM} \quad (15)$$

$$= \frac{(\tau_V^{\rm BC} + \tau_V^{\rm ISM}) m_{\rm d}}{\sigma_{\rm d}\xi Z} \quad (16)$$

$$= \frac{\tau_V m_{\rm d}}{\sigma_{\rm d}\xi Z}. \quad (17)$$

Brinchmann et al. assume that the dust grains correspond to Galactic-type dust and adopt a mass-weighted mean grain radius of $a = 0.14$ μm, based on Spitzer et al (1978). Since we assumed forward scattering, $\sigma_{\rm d} \approx \pi a^2$ and $\rho_{\rm d} \approx 3$ g cm^{-3}, which is the mean mass density of silicates and graphite grains (Spitzer et al 1978). This yields

$$\mu_{\rm gas}^{\rm c} = \frac{0.3\cdot 1.4\cdot 4\pi\cdot 10^{-15}}{\pi\cdot 10^{-14}\cdot \xi Z}\ {\rm g\ m}^{-2} \quad (18)$$

$$= \frac{0.3\cdot 0.56}{\xi Z}\ {\rm g\ m}^{-2} \quad (19)$$

$$= 0.2/(\xi Z)\ {\rm M}_\odot {\rm pc}^{-2} \quad (20)$$

Hence we can estimate $\mu_{\rm gas}$ from τ_V , using

$$\mu_{\rm gas} \approx 0.2\frac{\tau_V}{\xi Z}{\rm M}_\odot {\rm pc}^{-2} \quad (21)$$

[4]Note that CF00 denote this quantity as μ.

The main adjustable parameters for CL01 are Z, ξ, τ_V, U, t, β and the star formation history (SFH). Here, U is the ionization parameter at the edge of the Strømgren sphere., i.e. the ratio of ionizing-photon to gas density and β[4] is the fraction of the total effective absorption optical depth in the neutral ISM contributed by the ambient ISM. Recall that we know from Charlot & Fall (2000) that β is typically $\frac{1}{3}$. For our calculations, we assume the SFH to be constant and that $t = 10^8$ yr. We calculated 2×10^5 models, varying Z, ξ, τ_V and U over a certain range, as indicated in table 1. The models make up a model grid, which we use to fit our data to.

3.2 How the model works

To illustrate how the model works, we show different line ratio diagrams, in which the effect of varying the adjustable parameters mentioned above is demonstrated. Figure 4 and 5 show (parts of) the model grid in the plane of [NII]λ6584/Hα and [OIII]λ5007/Hβ. On the background we show a two-dimensional histogram of the star-forming galaxies in the SDSS sample with SNR>5 in the plane of those two line ratios. The [OIII]λ5007/Hβ ratio can be used as a measure for ionization and electron temperature (T$_{\rm e}$, the energy of electrons in the gas), which is explained below. The [NII]λ6584/Hβ ratio is a measure for metallicity, because [NII]λ6584 scales quadratically with the metallicity (Charlot and Longhetti 2001). Finally, figure 6 will show how the model works for τ_V, indicating the model grid and the star-forming galaxies in the plane of [NII]λ6584/Hα and Hα/Hβ. The latter is the line ratio that is used to calculate dust abundance in galaxies. This is explained in further detail in section 4.

3.2.1 U and ξ

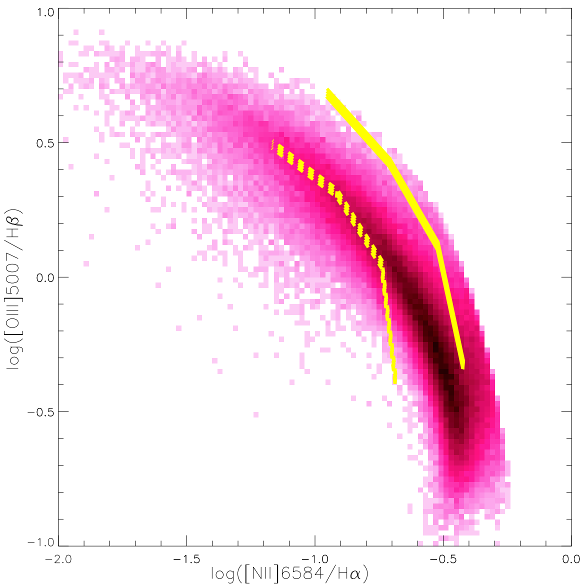

Figure 4: We display the model grid in the plane of two line ratios: [OIII]λ5007/Hβ versus [NII]λ6731/Hα. At the background, the SDSS star-forming galaxies are indicated by a two-dimensional histogram. Along the lines, the ionization parameter, U, is varied, increasing from -4 to -2 as the line goes up. The two different lines represent different values for ξ: the straight line shows the maximum value for ξ in our model grid, ξ=0.5, the dashed line indicates the minimum value, ξ=0.1.

In figure 4 we show the part of the model grid for solar metallicity ($Z = Z_{\odot}$=0.019). Along the lines, the ionization parameter, U, is varied, increasing as the line goes up. The two different lines represent different values of ξ: the straight line shows the highest value of ξ in our model grid, ξ=0.5, the dashed line indicates the lowest value, ξ=0.1. On the background we show a two-dimensional histogram of the star-forming galaxies in the SDSS sample with SNR>5.

Increasing U has the immediate effect of making high-ionization lines, like [OIII]λ5007 stronger. Therefore the [OIII]λ5007 /Hβ ratio can be used as a measure for ionization. Physically, increasing U means causing gas to be more concentrated in the inner parts of the birth clouds, where there is more ionization by stars (Charlot & Longhetti 2001).

The effect of the dust-to-metal ratio is model dependent. In CL01, the following process takes place: Increasing ξ means more oxygen gets depleted onto dust grains, reducing the amount of oxygen in the gas phase. Nitrogen, sulfur and neon are expected not to be depleted. Oxygen is an important coolant (Stasińska 1980). If it gets removed from the gas, cooling becomes less effective and the electron temperature increases. At low T_e , electrons have a low energy and they will evacuate their energy through low-ionization lines, in the infrared region of the spectrum. Increasing their energy will make them evacuate their energy more through optical transitions (Shields and Kennicutt 1995). Therefore, although oxygen is depleted, the amount of [OIII]λ5007 excitation increases. There will also be more [NII]λ6584 excitation.

3.2.2 Z

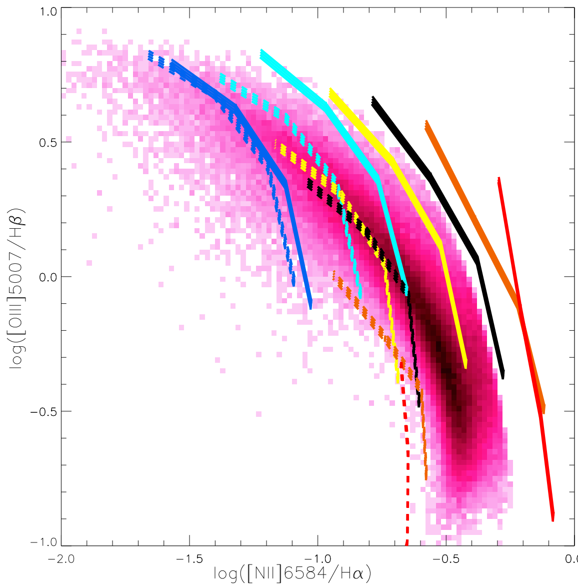

Figure 5: We show the model grid in the plane of two line ratios: [OIII]λ5007/Hβ versus [NII]λ6731/Hα. As the lines increase, U increases and the difference between straight and dashed lines is as indicated in figure 4. Different values for Z are shown, blue being the lowest value and red the highest, as indicated in table 1.

Figure 5 reveals what happens when the metallicity is varied, by showing the entire model grid. The blue lines indicate the minimum value of Z, whereas the red lines indicates the maximum value of Z, as indicated in table 1.

A first effect of increasing Z is that the metal lines get stronger. Looking at figure 5, this is easily spotted, since the [NII]λ6584/Hα ratio increases. We see that increasing Z slightly at fixed ξ also increases [OIII]λ5007 . However, metals contribute to cooling. With increasing metallicity, the electron temperature drops. This will make the high-ionization lines weaker. This is most prominently seen in the [OIII]λ5007 line, because it is an important cooling line at low Z. At high Z (oxygen abundances above 10^{-3}), cooling is efficient and the energy of the electrons is low. As explained above, energy will be evacuated through low ionization lines, in this case the [OIII]λ88μm line, hence the [OIII]λ5007 line weakens. Therefore the [OIII]λ5007/Hβ ratio can be used as a measure for T_e.

Note that Z also has an important effect on the influence of the dust-to-metal ratio. At low Z, the effect of ξ is minimal, because there is already very little cooling and a low oxygen abundance. The influence of ξ on cooling is much larger at high Z. The fact that the

[OIII]λ5007/Hβ ratio increases considerably, indicates that at high Z, increasing ξ affects the electron temperature substantially. At high Z, raising ξ increases the [OIII]λ5007/Hβ ratio considerably. Because the metal abundance is higher, this makes good sense. Since increasing ξ is effectively taking away more oxygen from the gas, at higher Z, a larger amount of oxygen is depleted, hence increasing T_e.

Because of the fact that the influence of ξ at cooling is much larger at high Z, it should be much easier to constrain ξ at high Z than at low Z. Since there is a larger separation between the models, obtaining a probability distribution function that has a well-defined peak should be feasible at high Z.

3.2.3 τ_V

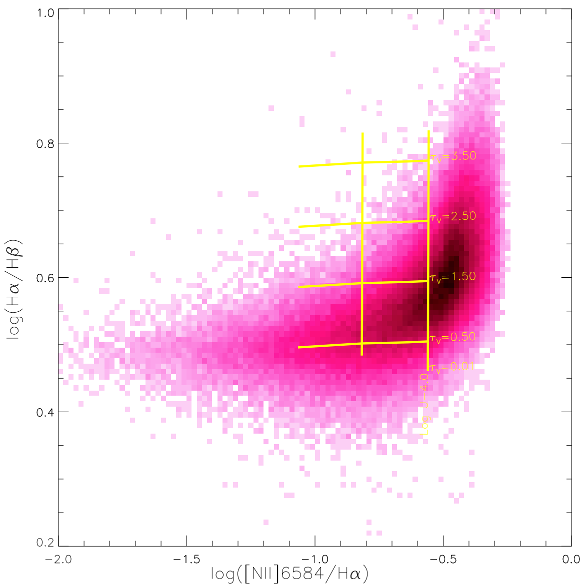

Figure 6: We show the model grid in the plane of two line ratios: Hα/Hβ versus [NII]λ6731/Hα. Hα/Hβ is a measure for dust abundance. Therefore this ratio is useful to show the effect of varying τ_V. The part of the model grid for $Z = Z_\odot$ is shown. Indicated are the different values for τ_V. We see that increasing the amount of dust results in more dust attenuation.

In figure 6 we show the part of the model grid for $Z_\odot$. Indicated are the different values for τ_V .

When there is more dust in a galaxy, the dust attenuation increases. Dust removes blue light more than red, so blue lines will be more attenuated than red lines. Therefore Hβ will be more attenuated than Hα, which increases the Hα/Hβ ratio (see figure 6). Hhence Hα/Hβ is often adopted as a measure for dust.

3.3 Fitting models to data

In order to get gas content estimates, we fit our samples of star-forming galaxies to the CL01 models. Usually the best fit model is determined by applying the method of the least squares. However, because of the large number of models, there could easily be a model that coincidentally fits best to a galaxy, whereas other models that only differ slightly from the obtained best-fit model, would not at all be a good approximation. Hence, the best-fit model that was found by using the method of least squares, might not at all be a good approximation for the galaxy, since there does not seem to be a physical foundation for the obtained best-fit.

We solve this problem by not using the method of the least squares, but by using a Bayesian approach (Kauffman et al. 2003, Brinchmann et al. 2004). To each model we assign a probability distribution $P(U, \xi, \tau_V, Z) = e^{-\chi^2/2}$. χ^2 is computed by minimizing

$$\chi^2 = \sum_i \frac{(F_i - AM(U, \xi, \tau_V, Z))^2}{\sigma_{F_i}^2}, \qquad (22)$$

where A is a scale factor for normalizing the total probability to unity, $M(U, \xi, \tau_V, Z)$ is the model grid with its adjustable parameters, F_i is the observed flux and σ_{F_i} is the corresponding uncertainty.

We are interested in the probability of the separate variables, e.g. $P(Z)$. In order to obtain those, we need to marginalize, i.e. sum over the other parameters:

$$P(Z) = \sum_U \sum_\xi \sum_{\tau_V} P(U, \xi, \tau_V, Z) \qquad (23)$$

This way we calculate probability distributions for all parameters, from which we can calculate various quantiles q_x, such as the median, i.e. the 0.5 quantile, and the 0.16 and 0.84 quantiles. The last two are used to calculate the uncertainties:

$$\sigma = \frac{q_{84} - q_{16}}{2} \qquad (24)$$

We assume that our median values are our best-fit values for the four parameters we vary.

In order to get physically meaningful results, we need our probability distribution functions (PDFs) to have a well-defined peak (i.e. resemble a gaussian), because then the median value will be the most probable value. To accomplish this, one needs to have enough information to get good constraints on the desired parameter. In our case, this means that we need enough emission lines. In figure 7 we show the effect that adding lines has on the PDFs. We start with [OII]λ3727 and show the PDFs for the indicated parameters as we add emission lines. The reader will immediately see that the PDFs become more like gaussians everytime a line is added. Note that ξ usually is badly constrained. ξ can only be well-constrained at high metallicity.

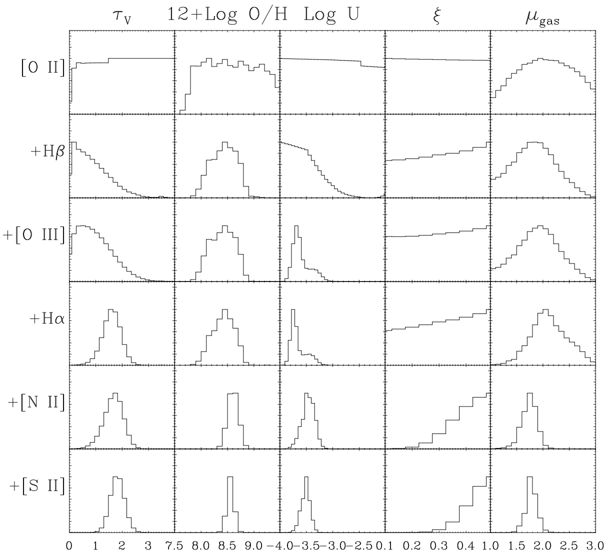

Figure 7: This figure shows the effect of adding information to a calculation of PDFs for the parameters we study. The top row shows the PDFs when only one line is available. We see that for most parameters, this results in a uniform distribution, indicating that there is no constraint on the values for the parameters. Moving down row by row, we add another line, increasing the amount of information. This results in PDFs with a well-defined peak, except for ξ, which will always be hard to constrain, unless the metallicity is very high.

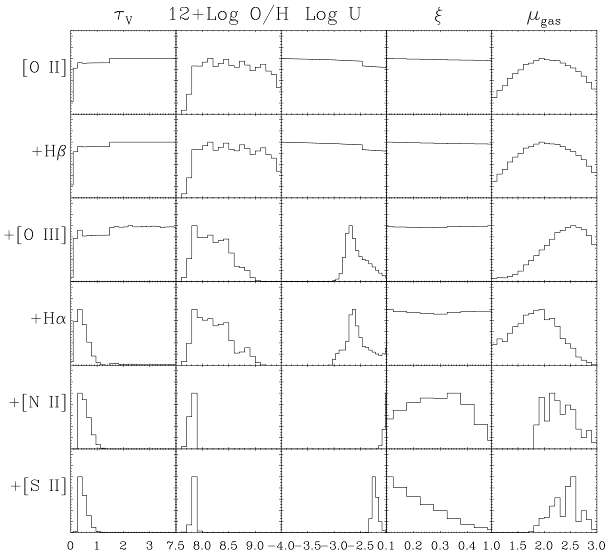

Figure 8: This figure shows the PDFs of different parameters, adding lines to constrain the different parameters as indicated in figure 7, for a typical Pea-object.

We fitted the CL01 model grid to the Pea-spectra and compared the best-fit values for 12+log(O/H), τ_V and U for the Peas, to the best-fit values of the small sample of 100 galaxies. We did this examination by eye, comparing the PDFs for both samples. In figure 8, PDFs for a typical Pea are shown. Comparing this to figure 7, the reader will immediately see the difference for the PDFs for τ_V, 12+log(O/H) and U. We discovered that in comparison to the galaxies of the small sample, Peas have very high ionization parameters, low values for the dust attenuation, and lower metallicities than ordinary galaxies. This is a first result for the Pea objects, further research is needed to study how these galaxies evolved to have these unfamiliar properties.

3.4 First application of the models: pea objects

To get a better understanding of how to use the models, we test them for a sample of galaxies in the SDSS that have very extreme properties. For this we use a sample of galaxies, that have recently been discovered amongst the large amount of SDSS galaxies. They stand out, because they have weird spectra, with very strong high-ionization lines. They have a very high equivalent width of the [OIII]$\lambda\lambda$4959, 5007 doublet (EW([O III])>500Å, York et al. (in prep.)) . The term was at first, and maybe still, humourously applied to objects that appeared green. More generally, all sorts of colours of Peas were found, the main criterium being that they should have a high ratio between the [OIII] emission line flux and broad band flux.

4 Tests for the gas surface mass density equation

We like to test the fitted parameters we calculated. Especially the values for $\mu_{\rm gas}$, because we will use this parameter in all our calculations. We compare our values to the values found by Leroy et al (2008). Leroy et al. used CO emission lines as a tracer for molecular HI gas and the 21 cm line . The result can be seen in figure 9 Here the column densities of stars are plotted against the ratio of the gas column density $\mu_{\rm gas}$ and the column density of stars μ_*, which from now on will be called $r_{\rm gas}$. The grey dots represent the results found by Leroy et al. The coloured dots represent the results for our small sample. We can see that for small $r_{\rm gas}$ values and high μ_* the galaxies overlap, but as soon as $\log(\mu_*) \lesssim 2.5$ and $r_{\rm gas} \gtrsim -0.4$ we see a discrepancy. We also plotted the uncertainties. It can clearly be seen that the uncertainties are not big enough to explain the discrepancy.

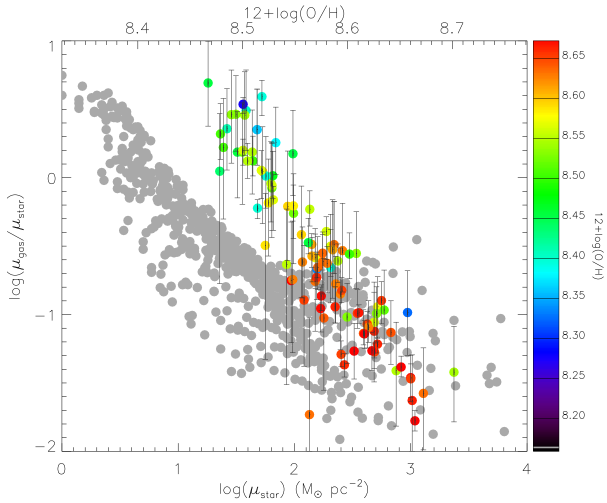

Figure 9: The values for $\mu_{\rm gas}/\mu_*$ plotted against the column densities of stars. The grey dots represent the results found by Leroy et al. The coloured dots represent the results for our small sample. We can see that for small $r_{\rm gas}$ values and high μ_* the galaxies overlap, but as soon as $\log\mu_* < 2.5$ and $r_{\rm gas} > -0.4$ we see a discrepancy.

We first assume that the values for the surface mass density of stars are correct (Brinchmann et al. 2004).

We then tested whether there is a redshift dependance. It is possible that the galaxies that lie above the galaxies of Leroy et al. have a higher redshift. This higher redshift may cause a higher value for $\mu_{\rm gas}$ than estimated for lower redshift, because of the aperture fiber of the SDSS. For higher redshift the greater part of the galaxy or the whole galaxy will fall inside the fiber aperture and this might increase the estimates of $\mu_{\rm gas}$. The SDSS will take a spectrum from the center of the galaxy. Gas is not equally distributed over the galaxy. The values of $\mu_{\rm gas}$ at the center of the galaxy (the bulge) might be different from the values at the edges (the gas surface mass densities can be higher at the edges). We did not find such a redshift dependency for the galaxies that deviate from the Leroy sample.

The discrepancy might be caused by the $\mu_{\rm gas}$ equation. It can be that this equation is incorrect or insufficient. We test whether we can change the parameters to bring our estimates of $\mu_{\rm gas}$ in agreement with that of Leroy et al. (2008). We remind the reader of our $\mu_{\rm gas}$ estimator:

$$\mu_{\rm gas} = 0.2\frac{\tau_{\rm V}}{\xi Z}{\rm M}_\odot{\rm pc}^{-2}. \tag{25}$$

We first tested the Z parameter. The oxygen abudance is used as a measure for the metallicity, because oxygen is the most abundant metal. However not only oxygen lines are used to determine the metallicity, also ratios with higher ionization lines, such as [NII], can be used. There is no generally accepted method to estimate oxygen abundances and significant differences can be found between methods as discussed in detail by Kewley & Ellison (2008). In figure 9 we show how the oxygen abundance varies in the relation. We can see that the galaxies that deviate from the Leroy sample have oxygen abundances below solar oxygen abundance. (An abundance of 8.67 is usually assumed to be the solar oxygen abundance. Brinchmann et al. 2004) Therefore we investigated whether there is a relation between the oxygen abundance and μ_*. This could be of importance because $r_{\rm gas}$ also depends on μ_*. However we did not find such a relation. Subsequently we tried to substitute a different value for the oxygen abundance and thus change the values for $\mu_{\rm gas}$. We did this in the following way:

$$\mu'_{\rm gas} = \mu_{\rm gas}\frac{\rm Z_{CL01}}{\rm Z_{other}} = \mu_{\rm gas}\frac{\rm (O/H)_{CL01}}{\rm (O/H)_{other}} \tag{26}$$

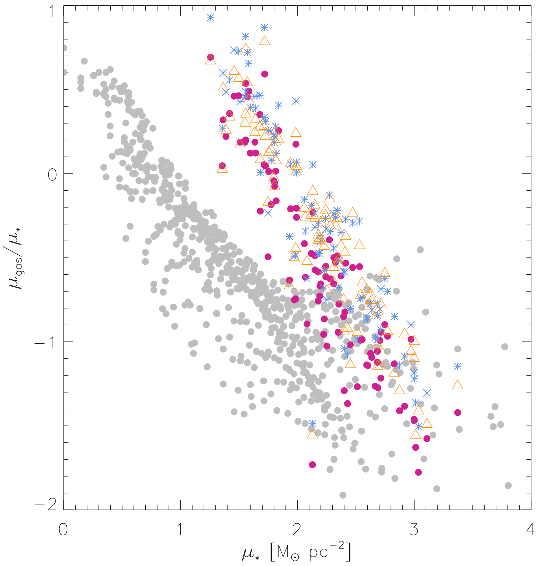

Figure 10: The purple dots indicate the oxygen abundances derived from CL01 the blue stars indicate mixed oxygen abundances. The orange triangles indicate oxygen abundances derived from the [NII]λ6584 /Hα ratio (Pettini & Pagel 2004)

This other oxygen abundance can be the 12+log(O/H) estimate derived from the ratio of [NII]λ6584 /Hα (Pettini & Pagel 2004):

$$12 + \log({\rm O/H}) = 8.9 + 0.57\cdot\log([{\rm NII}]\lambda6584/{\rm H}\alpha) \tag{27}$$

We also substituted an oxygen abundance that mixes several methods (see also Brinchmann, Kunth & Durret 2008). The results for the adjusted $\mu_{\rm gas}$ are showed in figure 10. We can see that the adjusted oxygen abundances only make matters worse.

Then we tested the $\tau_{\rm V}$ parameter. The CL01 models assume $\tau_{\rm V} \propto \lambda^{-0.7}$. Wild et al. (2007) assumes $\tau_{\rm V} \propto \lambda^{-1.3}$. With these assumptions we derive a new value for $\tau_{\rm V}$ in the following way.

$$\frac{\mathrm{H}\alpha}{\mathrm{H}\beta} = \left(\frac{\mathrm{H}\alpha}{\mathrm{H}\beta}\right)_0 \mathrm{e}^{-(\tau_{H_\alpha} - \tau_{H\beta})} \quad (28)$$

Where $\left(\frac{\mathrm{H}\alpha}{\mathrm{H}\beta}\right)_0$ is the true flux which has the value of 2.86. $\frac{\mathrm{H}\alpha}{\mathrm{H}\beta}$ is the observed flux. We use the ratios of Hα and Hβ because this is a good measure for the dust attenuation (this is explained in further detail in section 5). To calculate $\tau_{H_\alpha} - \tau_{H\beta}$ We use the following equation from Wild et al. (2007).

$$\frac{\tau_\lambda}{\tau_V} = (1-\beta)\left(\frac{\lambda}{5500\text{Å}}\right)^{-1.3} + \beta\left(\frac{\lambda}{5500\text{Å}}\right)^{-0.7} \quad (29)$$

Recall from section 3 that β is 0.3, τ_λ is the attenuation of a certain emission line (here we use Hα and Hβ). From this equation we can calculate the value of the ratio:

$$\frac{-(\tau_{H_\alpha} - \tau_{H\beta})}{\tau_V} = -0.3276 \quad (30)$$

Now using eq. 28 we can calculate:

$$\frac{\mathrm{H}\alpha}{\mathrm{H}\beta} = 2.86 e^{0.3276 \tau_V} \quad (31)$$

So the new value for the dust attenuation is:

$$\tau_V = \frac{1}{0.3276}\left(\frac{1}{2.86}\frac{\mathrm{H}\alpha}{\mathrm{H}\beta}\right) \quad (32)$$

Where the fraction of Hα and Hβ are the observed fluxes.

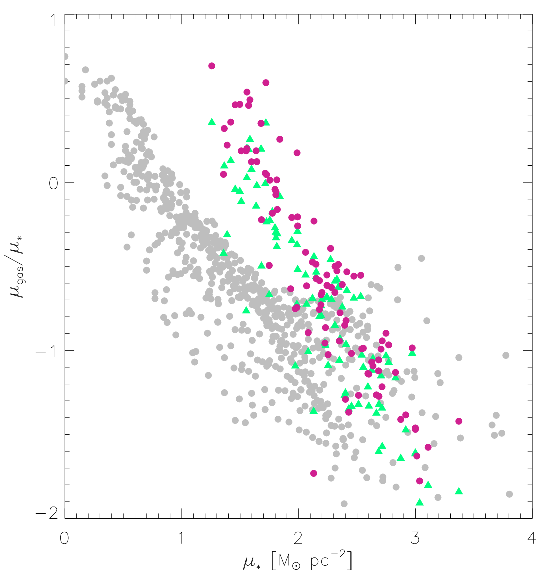

Figure 11: μ_{gas}/μ_* plotted against the column densities of stars, as indicated in figure 9. We see that for the adjusted values of τ_V, the discrepancy between the results of Leroy et al. and our sample decreases, though not enough to explain the discrepancy by adjusting τ_V.

The result for this new τ_V value is shown in figure 11 We can see that this new value of τ_V does not explain the deviation. The galaxies lie slightly lower on the relation but not low enough to make a difference.

So far we find no incorrect parameters for the μ_{gas} equation. A possible explanation for the deviation is that there is a missing gas component (i.e. tracer of cold HI or H2 gas) which Leroy et al. did not detect (Bernard et al. 2008) that causes the deviation. It is often argued that CO emission does not trace the molecular gas properly, for two reasons. First, CO molecules are more easily photodissociated than H2 and could be destroyed in diffuse H2 clouds. Second, the CO line is optically thick and its emission could be biased toward warm regions (Neininger et al. 1998). The discrepancy is also found by Meixner et al. (2009) where the same results where found for the Large Magellanic Cloud. We could also try to adjust the ξ parameter and the 0.2 prevalue of the μ_{gas} equation, but it is outside the scope of this project to discuss this in further detail.

5 The minimum set of emission lines

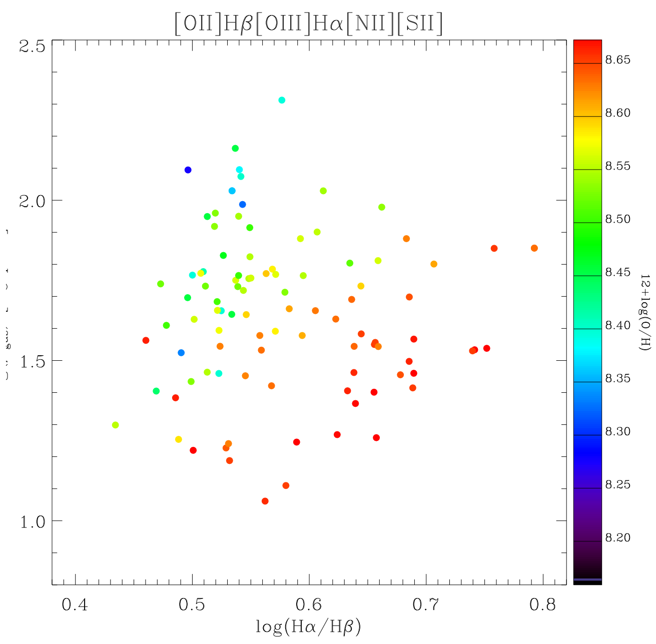

Figure 12: μ_{gas} vs. log(Hα/Hβ). Here we used all lines to estimate μ_{gas}. the different colours correspond to different oxygen abundances (12+log(O/H)). The log(Hα/Hβ) is a measure for the dust attenuation τ_V. From this trend we can see that when the dust attenuation increases, the amount of gas increases (gas scales linearly with dust). Galaxies with lower oxygen abundances clearly have less dust and more gas.

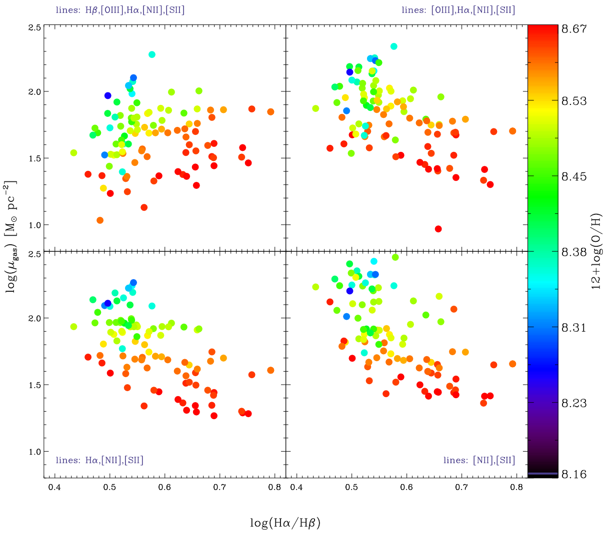

Figure 13: μ_{gas} vs. log(Hα/Hβ), see figure 12. Here we remove the blue lines as indicated. The different colours correspond to different oxygen abundances (12+log(O/H)). Removing [OII] does not affect the trend much, but with removing Hβ the trend disappearse, because we can not constrain τ_V anymore.

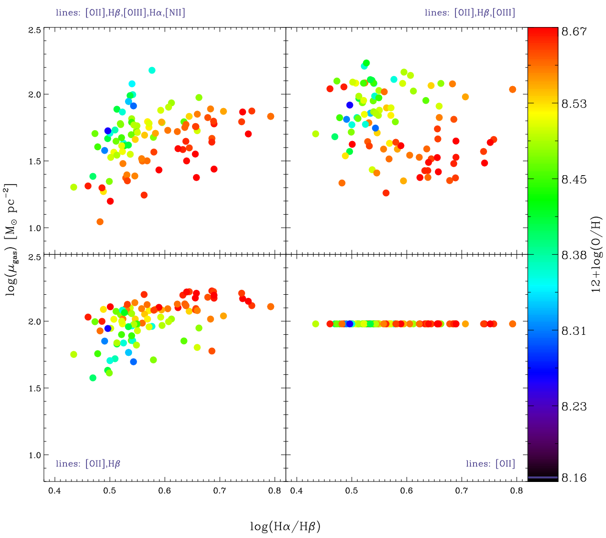

Figure 14: μ_{gas} vs. log(Hα/Hβ), see figure 12. Here we remove the red lines as indicated. The different colours correspond to different oxygen abundances (12+log(O/H)). For removing [SII] the trend is retained. When removing [NII] and Hα (can only be removed together because they lie so close together in the spectrum) the trend disappears. When only [OII] is left there is no trend at all.

We used the 6 strongest emission lines to calculate the values for the parameters, namely [OII]λ3727, H$\beta\lambda$4861, [OIII]λ5007, H$\alpha\lambda$6563, [NII]λ6584 and [SII]λ6731. [OIII]λ5007 is actually one line from the [OIII]$\lambda\lambda$4959, 5007 doublet. Because both lines will give the exact same information, it would not make any difference which emission line from the doublet is used, or whether they are both used to estimate $\mu_{\rm gas}$ (Osterbrock & Ferland 2005). Therefore we only use [OIII]λ5007 in our study. For particular observations it can be possible that not all of these lines are available. For example, if we observe at high redshift, we may not be able to observe the reddest lines in our sample. Ideally an optical spectrograph can cover a wavelength range of [3800Å, 1μm]. At a redshift of $\approx$0.5 we can not observe the reddest line [SII]λ6731 anymore and at a redshift of $\approx$1.7 we can not observe [OII]λ3727 anymore. Another difficulty emerges at the other end of the optical part of the spectrum. For galaxies at very low redshift it might not be possible to observe the [OII]λ3727 line. This line needs to have a redshift of z $>$ 0.02 to be observed by the SDSS. Furthermore when you observe at higher redshift the survey is likely to be optimized for the red wavelength region. There may be a limited spectral coverage, so if there are still blue lines to observe with a wavelength outside the range of the spectrograph, these lines will be unobservable. We can therefore conclude that it is very likely that we will not always be able to observe all the lines which we use to constrain the value for $\mu_{\rm gas}$ using an optical spectrograph.

We investigate how many lines we can omit and still get a physical meaningful result. We start with the 6 strongest lines emission lines: [OII]λ3727, H$\beta\lambda$4861, [OIII]λ5007, H$\alpha\lambda$6563, [NII]λ6584 and [SII]λ6731. First we will remove lines with the highest wavelengths (simulating what will happen when moving to higher redshift) and then we will remove the lines with the lowest wavelengths. This approach results in 11 different line sets.

There are two ways to investigate what happens to the parameters when lines are left out of the estimates. The most obvious way is to investigate how the probability distribution functions (PDFs) change when we omit lines. In figure 15 we show what happens for the different PDFs of $\mu_{\rm gas}$ we got from the fit of a typical galaxy. The changes in the PDFs show us that when lines are removed the width of the distribution increases, so the uncertainty increases. The blue lines indicate removing blue lines and the red lines indicate removing red lines. It is clear that $\mu_{\rm gas}$ is not so well constrained when red lines are removed in comparison with removing blue lines.

Recall that $\mu_{\rm gas}$ depends on the $\tau_{\rm V}$, Z and ξ, which we get from the model grid. Therefore it is necessary to also evaluate the PDFs for these parameters. Figures 16, 17 and 18 show the PDFs of the dust attenuation $\tau_{\rm V}$, the metallicity Z and the dust to metal ratio ξ. We see, that lowering the amount of information, decreases the peaks in the distribution functions for $\mu_{\rm gas}$, $\tau_{\rm V}$, ξ and Z. This means that the estimates for the parameters become less well-defined and the uncertainty increases.

Another less obvious but more qualitative way is to look at trends. It is much easier to see what the physical meaning is to remove lines when we examine trends. The particular trend we look at shows us a relation between Hα divided by Hβ, μ_{gas} and the metallicity (see figure 12). The Hα/Hβ ratio is a measure for the amount of dust in a galaxy, because the effect of dust is to reduce the ionization rate and hence the luminosities of all H-recombination lines by a similar amount (Charlot and Longhetti 2001). The gas to dust ratio of a galaxy is usually given as a constant (Osterbrock & Ferland 2005), this means that dust scales with gas linearly. Increasing the amount of dust is increasing the amount of gas. Moreover, galaxies with lower oxygen abundances clearly have less dust and more gas.

In figure 13 we show what happens when we omit the lines from the blue side of the spectrum. Omitting the [OII]λ3727 line clearly does not affect the estimate much. However, leaving out one more blue line, H$\beta\lambda$4861, does not leave us with a physical relation anymore. Moving up in dust, but down in gas contradicts the relation mentioned above.

The following changes in the relation occur when removing red lines (figure 14) . Removing the [SII]λ6731 line does not have a large effect, the trend remains. Removing the [NII]λ6584 line weakens the oxygen abundance relation, but the trend in gas to dust is maintained. As expected, when the H$\alpha\lambda$6563 line is lost, the relation disappears, for there no longer exists enough information to constrain the dust attenuation. When [NII] is omitted Hα has to be omitted too, because the two lines are very close together in the spectrum.

5.1 Discussion of results

We conclude that the minimum set of emission lines is: [N II]λ6584, Hα, [OIII]λ5007 and/or [O III]λ4959 and Hβ. We could also use the [O III]λ4959 line, which would not make any difference, because both lines are equally strong. We can also conclude that we need both the PDF and the trend to come to this conclusion for the minimum set of lines. We examined more trends besides the trend mentioned above in figure 12. We used this trend to explain the effect of removing lines from the estimate because this trend shows the changes most clearly. This is a qualitative result. Our sample is too small for statistical analysis. It does however show a clear physical relation.

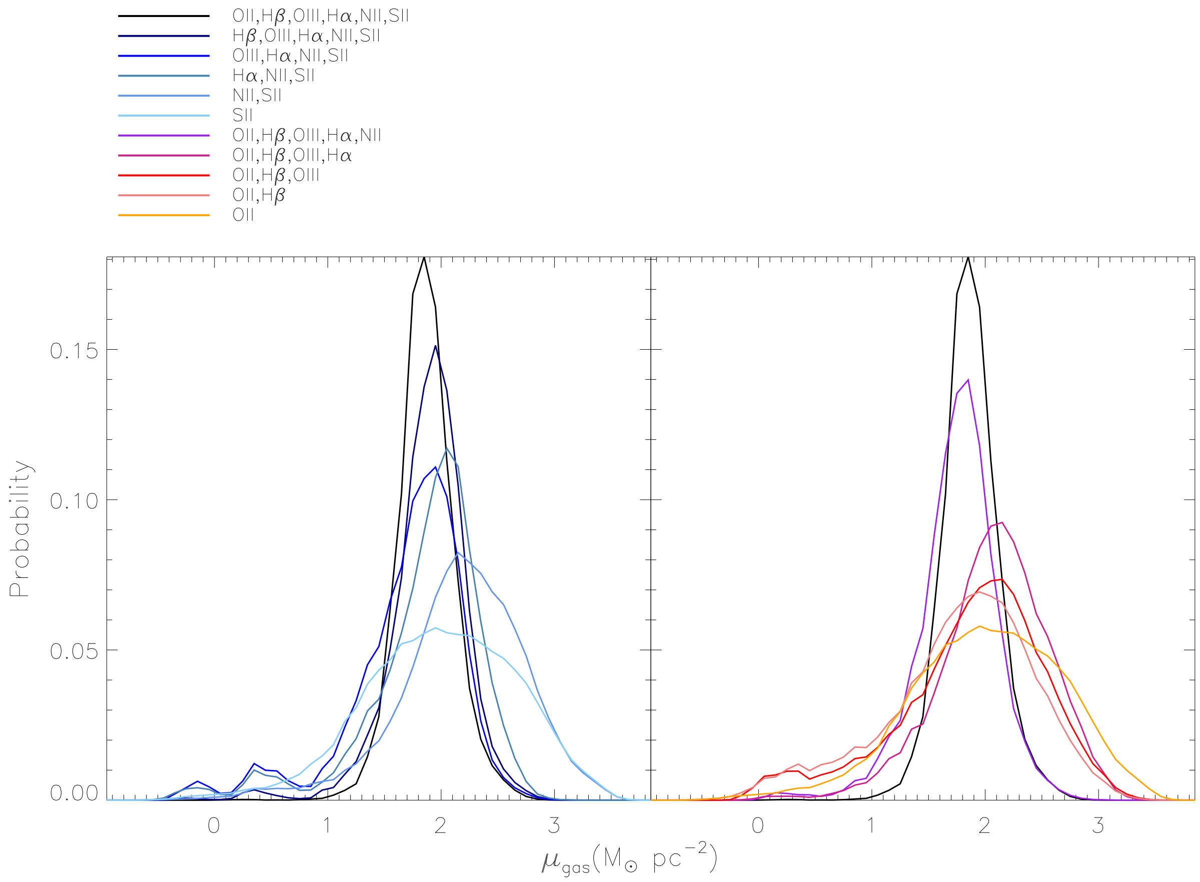

Figure 15: Here we show the different PDFs for μ_{gas} from a typical galaxy of Sample I. The changes in the PDFs show that the width of the distribution increases and the height of the peak decreases, when lines are removed. In this figure the red lines indicate the removal of lines from the red side of the spectrum, the blue lines indicate removal of blue lines from the spectrum. The The legend indicates which lines remain.

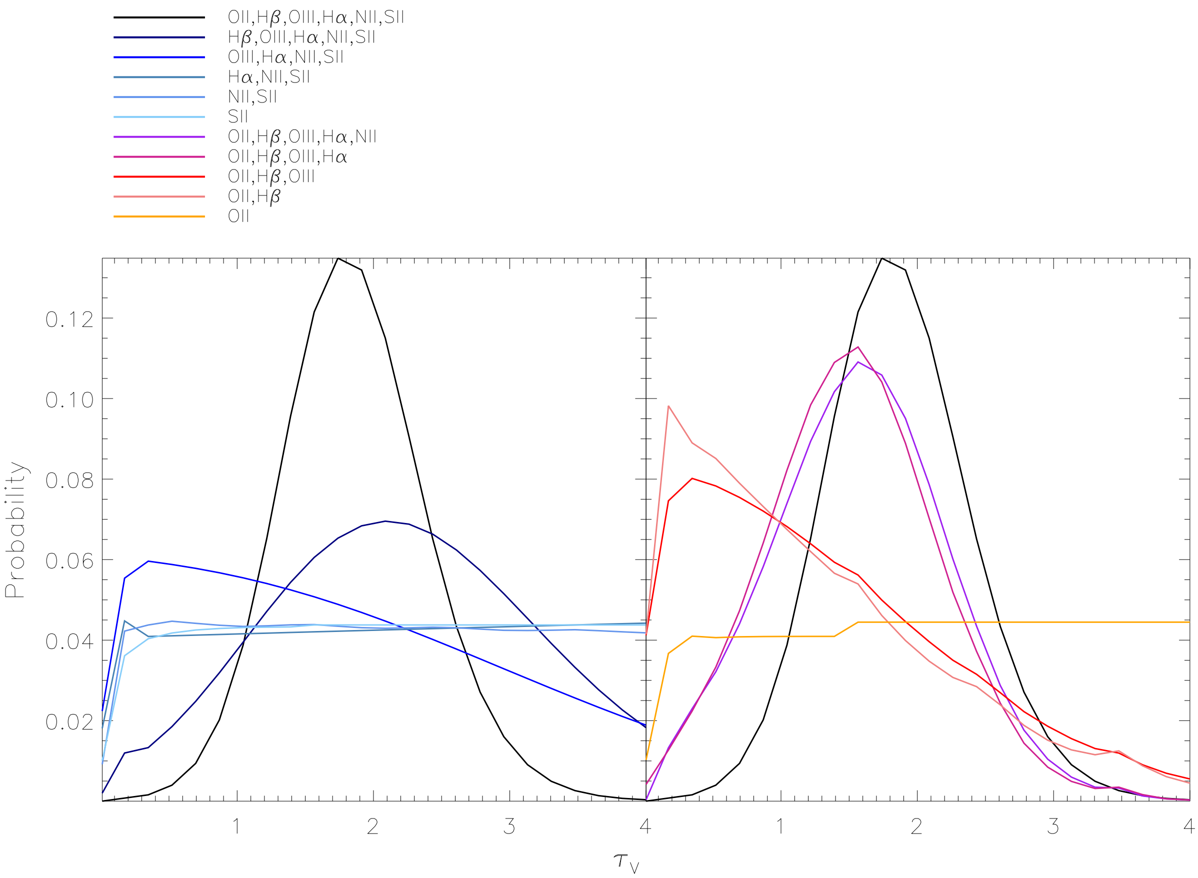

Figure 16: Here we show the different PDFs for $\tau_{\rm V}$ from a typical galaxy of Sample I. The changes in the PDFs show that the width of the distribution increases and the height of the peak decreases, when lines are removed as indicated in figure 15.

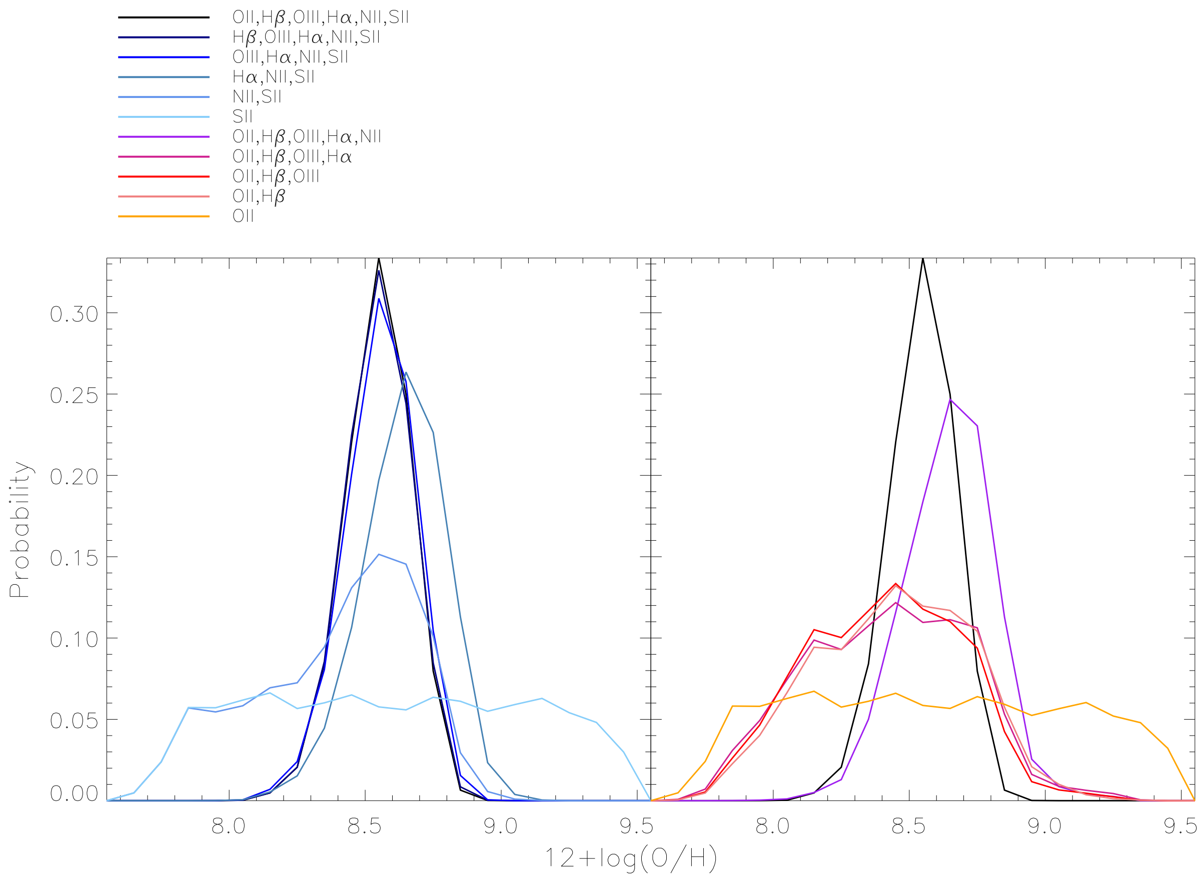

Figure 17: Here we show the different PDFs for the oxygen abundance from a typical galaxy of Sample I. The changes in the PDFs show that the width of the distribution increases and the height of the peak decreases, when lines are removed as indicated in figure 15.

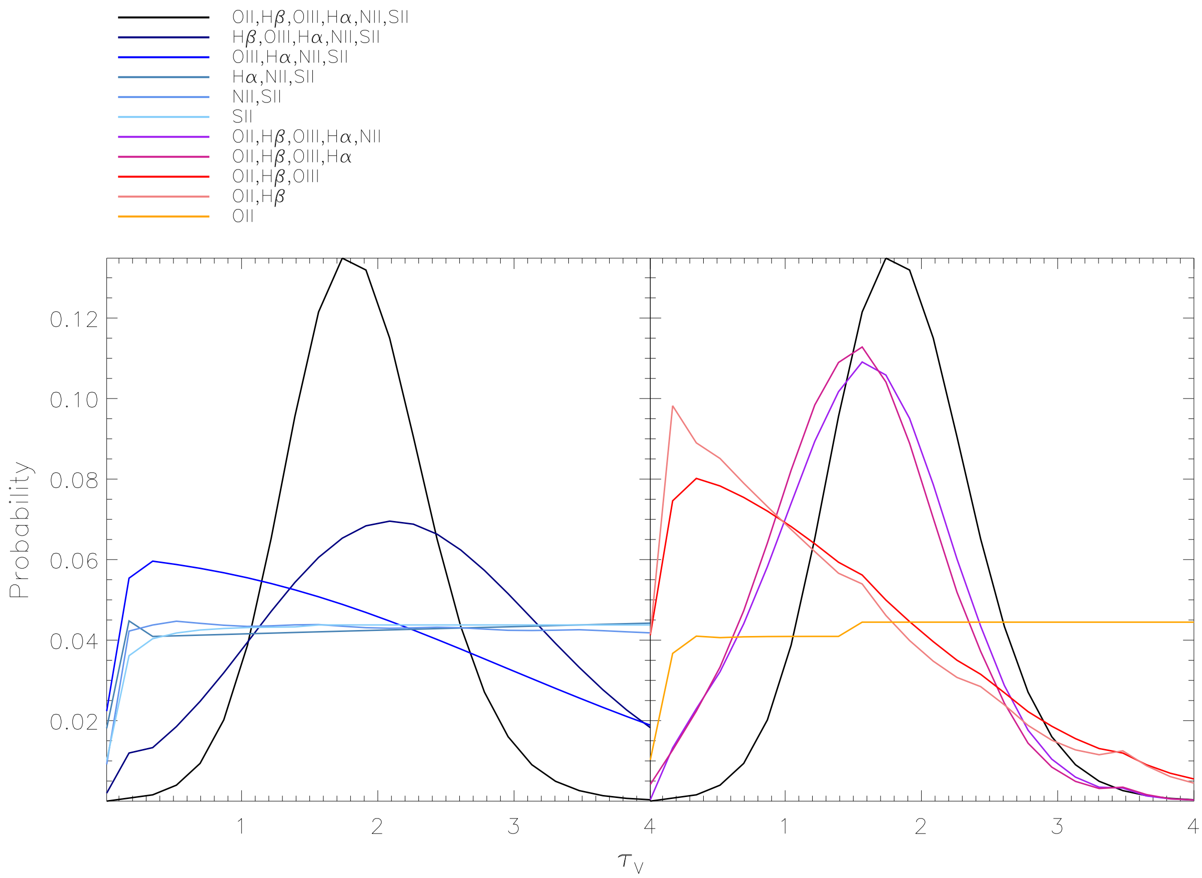

Figure 18: Here we show the different PDFs for ξ from a typical galaxy of Sample I. The changes in the PDFs show that the width of the distribution increases and the height of the peak decreases, when lines are removed as indicated in figure 15. We see that ξ is badly constrained, even with all lines present.

6 Application & results

We showed that we can get a physical meaningful result by using the following minimum set of emission lines: [N II]λ6584, Hα, [OIII]λ5007 and/or [O III]λ4959 and Hβ with SNR>5. Now we use a pre-existing dataset for $\mu_{\rm gas}$ and 12+log(O/H) that satisfy the criteria mentioned for Sample II in section 2. These estimates use at least the minimum set of emission lines.

6.1 The mass-metallicity relation

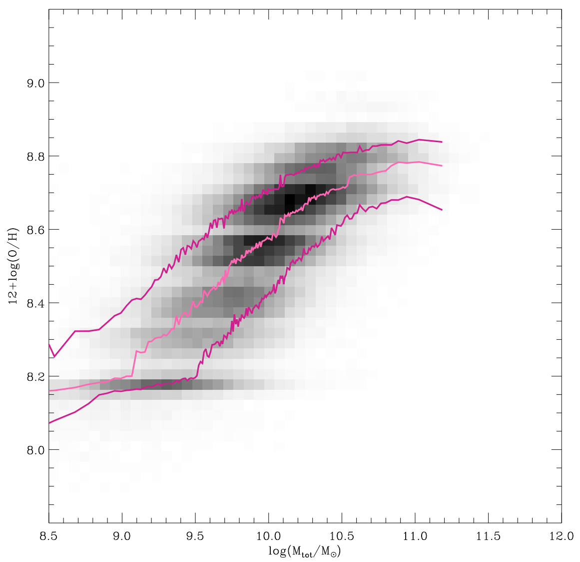

Figure 19: The mass-metallicity relation for our sample, shown by a two-dimensional histogram. The relation is shown by the median values calculated for mass bins, each of them containing 750 galaxies. This closely resembles the MZR as found by Tremonti et al. (2004), there is a ≈0.2-0.3 dex shift, due to a overall uncertainty in the calibration of the oxygen abundances. This also causes the dark lines in the bins. For further reference on the oxygen calibration, see Brinchmann et al. (in prep.).

We use the gas estimates to derive the gas content variation in the mass-metallicity relation (MZR; Tremonti et al. 2004 ; Zhang et al. 2009). The MZR for Sample II is shown in figure 19 . This relation is particularly interesting in studies of galaxy formation, because it reflects the fundamental role that galaxy mass plays in galactic chemical evolution. There is a striking correlation observed, indicated here by the median trend, which extends over two dex in mass and a factor of 5 in metallicity. The correlation is nearly linear for galaxies with masses from $10^9 M_\odot$ to $10^{10.5} M_\odot$ and after that a gradual flattening occurs. Unlike Tremonti et al. (2004), we use the total mass to show the MZR. The total mass of a galaxy is defined as:

$$M_{\rm tot} = M_{\rm gas} + M_*, \qquad (33)$$

where $M_{\rm gas}$ is the mass of the gas and M_* is the mass of stars in the galaxy. We calculate the total gas mass of the galaxy using:

$$M_{\rm gas} = M_* r_{\rm gas}, \qquad (34)$$

where $r_{\rm gas}$ is the ratio of gas mass to stellar mass:

$$r_{\rm gas} = \frac{M_{\rm gas}}{M_*} = \frac{\mu_{\rm gas}}{\mu_*}, \qquad (35)$$

where μ_* is the gas surface mass density of stars.

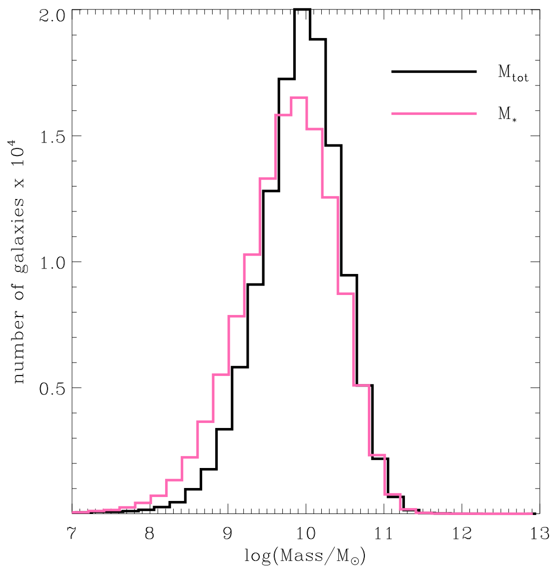

Figure 20: Histogram of the number of galaxies per mass-bin for the total mass and the stellar mass. If we assume a closed box model $M_{\rm tot}$ will be the same for the galaxy at all times, whereas the stellar mass and gas mass separately will change.

The values for the M_* and μ_* are calculated as in Kauffman et al. (2003). We use $M_{\rm tot}$ because it remains constant over time, whereas the stellar mass and gas mass change over time. Fig 20 shows a histogram of the number of galaxies per mass-bin for the total mass and the stellar mass. We see that the histogram for M_* is shifted towards lower mass, in comparison to the total mass, as one would expect. Now if the fraction of gas would be the same for each galaxy, the shift would be equal for all masses. This is however not the case. We see that the shift increases for lower masses, so low-mass galaxies must have higher gas fractions than high-mass galaxies.

Although there seems to be a tight correlation between mass and metallicity, the scatter around the relation does not come from errors, but from a spread in the data. The 1-σ spread in our data is 0.13 dex, which is indicated by the upper and lower lines in figure 19. Our goal is to understand what physical mechanism lies at the bottom of this spread.

6.2 Effective yield & closed box model

Following Tremonti et al. (2004) we assume that galaxies are closed box models (see also Pagel 1997). For this model we assume that no gas escapes from or is added to the galaxy, so the system has a constant total mass. At time t=0 all the mass of the galaxy is located in low metallicity gas. Furthermore we assume that the galaxy is well-mixed (it has the same composition everywhere) and the massive stars return their nucleosynthetic products rapidly, faster than the time it takes to form a significant amount of stars. The rate at which stars return their nucleosynthetic products is assumed to be constant in this model. This means that with time the metallicity will increase because high mass stars increase the metallicity rapidly, while the amount of gas will decrease due to star formation.

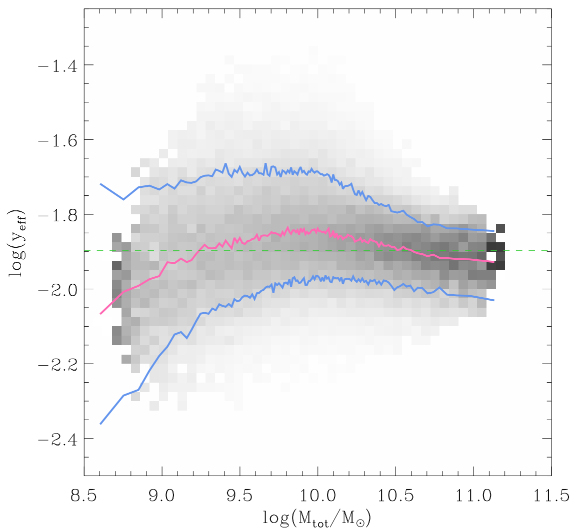

Figure 21: The effective yield versus M_{tot} for Sample II, shown in a two-dimensional histogram. The distribution function was normalized along the x-axis, so that the total number of galaxies in each bin is the same. This has the advantage of showing the relation more clearly. The pink line indicates the median trend, calculated in mass bins of 1000 galaxies. The blue lines indicate the 0.16 and 0.84 quantiles, where in between lies 68% of the data. The green line represents the true yield ($(2/3)Z_{\odot} \approx 0.02$, Pagel 1997)

To gain more insight into the mass-metallicity relation and to investigate whether the closed box model is correct, we explore the relation between the yield and total mass. Stellar yield (y), or true yield, is the amount of heavy elements produced and ejected by a generation of stars, as mentioned above. The metallicity depends on the stellar yield in the following way:

$$Z = y \ln(f_{\text{gas}}^{-1}), \tag{36}$$

where f_{gas} is the gas mass fraction, i.e. the gas mass divided by the total mass:

$$f_{\text{gas}} = \frac{\mu_{\text{gas}}}{\mu_* + \mu_{\text{gas}}} \tag{37}$$

If we assume that galaxies evolve as closed boxes, the yield is approximately constant in time and the metallicity is the same for every galaxy:

$$y = \frac{Z}{\ln(f_{\text{gas}}^{-1})} = constant \tag{38}$$

Now we show the yield as measured by observing oxygen abundances in figure 21. The true yield, which is equal to 2/3 times the solar metallicity ($Z_{\odot} \approx 0.02$, Pagel 1997) is also shown by the dashed line. We see that the median trend is well explained by a closed box model. Therefore we can assume that most galaxies evolve as closed box models. There is however a large spread around it, which cannot be explained by the closed box model. We want to understand what could cause this spread.

This leads us to define an effective yield (y_{eff}), which is not constant in time:

$$y_{\text{eff}} = Z(obs) \ln(f_{\text{gas}}^{-1}) \tag{39}$$

We can see that our median trend for the effective yield slightly exceeds the value of the true yield at $10^{9.3} M_{\odot} < M_{\text{tot}} < 10^{10.5} M_{\odot}$. This might be caused by the fact that we assume that what is measured within the fibre apertures is typical for the galaxies. Nearby galaxies will not be completely covered by the fibres, hence only the centre of those galaxies will be measured. For most galaxies though, one will find that there are larger gas fractions towards the edges of the galaxies. The gas at the edges might be less enriched than the gas in the centre. Therefore our values for the effective yield can be too large.

Another possibility is that the typical gas fractions are higher at $10^{9.3} M_{\odot} < M_{\text{tot}} < 10^{10.5} M_{\odot}$, and gas fractions decrease towards higher masses. This might cause the slight decrease in the median effective yield at masses higher than $10^{10.5} M_{\odot}$.

Note also that the median trend deviates from the true yield more towards lower masses. The median effective yield is considerably lower there. From that and the scatter in figure 21, we can conclude that we cannot assume a closed box model for our galaxies and there must be in- and/or outflow of gas.

6.3 The gas content variation in the MZR

Because y_{eff} depends on the gas fraction, we use f_{gas} to analyse the mass metallicity relation in further detail. We want to show how the gas fraction changes when we move up along the relation. f_{gas} is a useful quantity for showing how the galaxy has exhausted it's low metallicity gas, so we expect that the mass-metallicity relation will depend on this quantity. If we assume that a galaxy starts with only low metallicity gas, we can adopt the following equation:

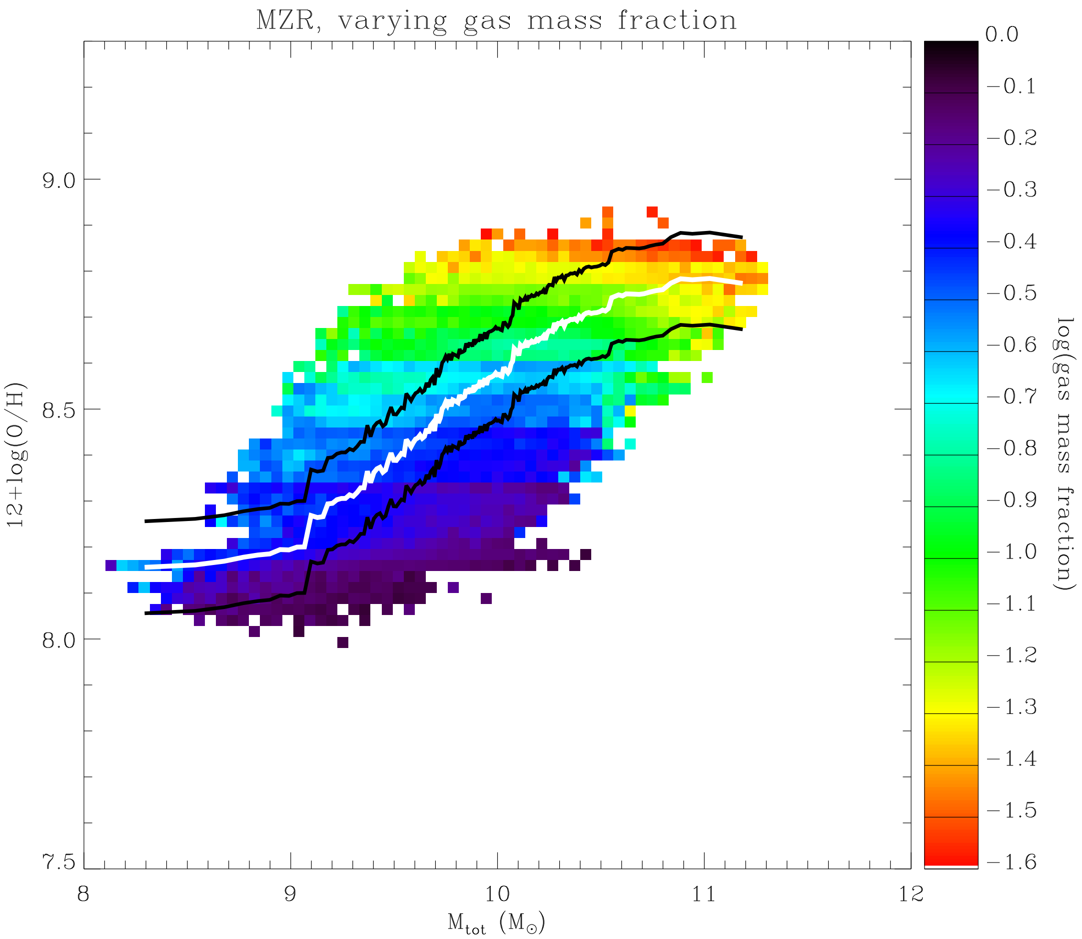

Figure 22: The gas-mass fraction variation in the mass-metallicity plane, for Sample II. The white line shows the median trend of the MZR, as in figure 19. This was calculated by calculating the mean oxygen abundances in mass bins of 750 galaxies. The black lines indicate where galaxies lie within 0.1 dex above or below the relation (i.e. the median trend). For our study, galaxies within these region are considered to be on the relation. The colours show the variation of $\log(f_{\rm gas})$ in the MZR plane. We see that at low metallicity, the gas fractions are high, as opposed to high metallicity. Note however, that there not only exists a metallicity dependency, but also a mass dependency. In order to derive the metallicity dependency, we need to remove the mass dependency. Therefore at fixed mass,

$$f_{\rm gas} = \frac{M_{\rm gas}}{M_{\rm gas} + M_*} \quad (40)$$

$$= \frac{M_{\rm gas}(t)}{M_{\rm gas}(0)} \quad (41)$$

$f_{\rm gas}$ (t) can also be seen as the fraction of gas mass at time t, divided by the total gas mass $f_{\rm gas}$ (0) the galaxy started with at time 0. Because this is equal to the fraction of gas mass divided by the total mass (mass of stars and gas, see figure 20), we know how much of the gas of the galaxy has been used to create stars, unless there has been a large inflow or outflow of gas, but we will consider this later.

In figure 22 we mapped the gas fractions of Sample II onto the mass-metallicity plane by means of colour coding, an approach also used by Zhang et al. (2009). The median trend of the mass-metallicity relation is shown by the white line. The two black lines indicate the galaxies 0.1 dex above and below the relation (the use of this indication will be explained later). The colours indicate the logarithms of the gas mass fractions. Increasing $f_{\rm gas}$ by only 0.3 dex, means doubling it. The gas fractions for our sample vary between -0.1 (violet) and -1.6 (red), indicating that the high-mass galaxies above the relation, have thirty times less gas than the low-mass galaxies below the relation. The gradient in $f_{\rm gas}$ tells us that $f_{\rm gas}$ decreases with increasing metallicity. Note however that the variation in $f_{\rm gas}$ not only depends on the metallicity. From figure 22 we also see that there is a mass-dependency. Zhang et al. (2009) found similar results.

We use the following method to show how the gas mass fraction changes with the metallicity. We see in figure 22 that there exists not only a relation between the metallicity and $f_{\rm gas}$, but also between $M_{\rm tot}$ and $f_{\rm gas}$. Low-mass galaxies have higher gas fractions than high-mass galaxies. This has as a consequence that we cannot immediately calculate the residuals of the oxygen abundance like Tremonti et al. (2004) did. To get the relation between the metallicity and $f_{\rm gas}$, we need to remove the relation between $M_{\rm tot}$ and $f_{\rm gas}$. First, we define that galaxies that lie on the relation $g_{\rm on}$ are the galaxies inside a range of 0.1 dex above and below the relation as indicated by the black lines in figure 22. The galaxies outside the relation $g_{\rm off}$ lie outside the black contours. Then we divide the relation into mass bins and for every mass bin, we subtract the median values of oxygen abundance for $g_{\rm on}$ from the oxygen abundances outside the relation. This gives us $\Delta(12+\log({\rm O/H}))_i$, the variation in metallicity per bin:

$$\Delta(12 + \log({\rm O/H})_i) =$$

$$12 + \log({\rm O/H})(g_{{\rm off},i}) - \langle 12 + \log({\rm O/H}(g_{\rm on}) \rangle \quad (42)$$

We want to compare this to the variation of $f_{\rm gas}$ and other parameters such as the gas surface mass density ($\mu_{\rm gas}$), the stellar surface mass density μ_* and the gas-to-stellar mass ratio ($r_{\rm gas} = \frac{\mu_{\rm gas}}{\mu_*}$). We calculate this variation the exact same way:

$$\Delta(x_i) = x(g_{{\rm off},i}) - \langle x(g_{\rm on}) \rangle, \quad (43)$$

where x can be any of the parameters mentioned above.

The results for this analysis are shown in figure 23. We plotted the median trend, indicated by the black line. The shaded regions indicate the 2-σ spread in data. The dashed line indicates where the variation is zero, i.e. where the values for the parameters do not deviate from the median values on the relation. A positive variation means that the values for the parameters are higher than the values on the relation. Negative values for the metallicity indicate galaxies below the relation i.e. lower metallicities; positive values indicate galaxies above the relation, i.e. higher metallicities. A clear trend can be seen for these parameters. We see that when the gas mass fraction increases, the metallicity decreases. Typically, when you double the amount of gas in a galaxy, the metallicity decreases with a factor of 1.5. Similar trends can be seen for $\mu_{\rm gas}$ and $r_{\rm gas}$. The trends continue above the median trend of the MZR. A plausible explanation for these results is, that galaxies that lie below the median trend of the MZR, have had recent inflow of metal-poor gas. This gas could come from its halo, or from interaction with another galaxy (see Ellison et al. 2008). The variation in gas above the MZR, indicating smaller gas fractions for systems that lie above the MZR, can be explained by outflow of gas. The galaxy could have ejected its gas further into its halo, where it might eventually rain back on the galaxy or escape into the intergalactic medium, where it is lost (see Garnett 2002; Tremonti et al. 2004).

We also show, that increasing μ_* has the effect of increasing the metallicity. This is reasonable, for a higher amount of stars will eject a higher amount of heavy elements into the ISM, which also supports the closed box model.

We also studied the variations of the parameters for low and high mass galaxies separately. This is shown in figures 24 and 25. The green lines indicate the average trend in the variation. We define our low-mass galaxies to have a mass of $8 < \log(M_{\rm tot}/M_\odot) < 9.5$ and high-mass galaxies to be in the range $\log(M_{\rm tot}/M_\odot) > 10.5$. We made those mass cuts, because there might be different physical processes going on in low-mass galaxies, compared to high-mass galaxies. Recall that we saw in figure 20 that the shift towards lower mass, was bigger for low-mass galaxies, indicating higher gas fractions. Also, the cut for high-mass galaxies was chosen deliberately for two reasons: $10^{10.5} M_\odot$ is the characteristic mass, i.e. the median value of the mass distribution of galaxies at the present day, as derived by Kauffmann et al.(2003). The second reason is that we recall from figure 21 that the median effective yield decreases slightly below the true yield, indicating that some unraveled process might be going on.

We see that for high-mass galaxies, the trend in variation of gas fraction and gas surface mass density is steeper, than for low-mass galaxies. The trend for the gas-star ratio is similar for both sub-samples, but the trend for the stellar surface mass density is flatter for high-mass galaxies. This means that for high-mass galaxies, which have lower gas fractions, if you increase the amount of gas, the metallicity does not decrease as much as it would for their low-mass counterparts. Also, increasing the stellar surface density will increase the metallicity for high-mass galaxies more significantly than for low-mass galaxies. This is an indication that inflow is more important for low-mass galaxies, because the effect of inflow is much larger on the chemical evolution of low-mass galaxies, than on their high-mass counterparts.

7 Summary and Conclusion

We derived the mass-metallicity we using a sample of 123488 star-forming galaxies from the SDSS Data Release 7, selected by criteria described in section 2, and oxygen abundances from Brinchmann et al. (in prep.). Although the correlation we derived is tight, uncertainties alone do not account for the spread in data.

To find possible explanations, we looked at the effective yield of our galaxies, i.e. the amount of heavy elements produced by stellar nucleosynthesis as observed in a galaxy. We compared this with the true yield, i.e. the amount of heavy elements produced in a galaxy that evolves in accordance with a closed box model (no in- or outflow of gas). We find that since the effective yield is not the same as the true yield (particularly for low-mass galaxies) and that there is a large spread in data, there might very well be in- or outflow of gas.

To further investigate this hypothesis, we derived the gas content variation in the mass-metallicity relation. In order to do that, we had to obtain estimates for the gas content. We derived gas surface mass densities using only optical emission lines and fitting spectra to a model grid, calculated from Charlot & Longhetti (2001). Their model is based on the stellar population synthesis code from Bruzual and Charlot (1993), the photoionization code Cloudy from Ferland (1996) and the model for attenuation by the interstellar medium introduced by Charlot & Fall (2000). We fitted our spectra using a Bayesian approach, hence calculating probability distribution functions for various parameters, that make up the gas content. We also applied the models in extreme parameter space, unleashing them on a subset of galaxies from the SDSS sample that have striking spectra. Those galaxies, humorously called Peas are not yet well understood. We find that they have very high ionization parameters, low metallicities and low dust attenuations.

To test the reliability of our estimates, we examined the required amount of emission lines needed to get good values for the gas content. For this investigation we used a small sample of a hundred galaxies, chosen to span the full range of mass and signal-to-noise in the spectrum. By looking at the trend between $\mu_{\rm gas}$ and Hα/Hβ, we determined what emission line are required to get a reliable estimate of $\mu_{\rm gas}$. We conclude that the minimum set of optical emission lines required to maintain physically meaningful results is: Hβ , [OIII]λ5007 , Hα , [NII]λ6584 . This gives us the minimum requirements for a larger galaxy sample, which we used for the mass-metallicity study.

We did however first test our values once more by comparing them to those derived by Leroy et al. (2008). We found that they are in good accordance at solar metallicity, but gas surface mass densities of galaxies with lower metallicities deviate from those of Leroy et al. We tested the parameters we used to calculate the gas surface mass density and they seem to be accurate. A possible explanation for the deviations is a missing gas component.

We derived the mass-metallicity relation for a sample of 123488 star-forming galaxies. We assumed closed box evolution for our galaxies, in order to explain the scatter in the MZR. To investigate whether the closed box model is a good approximation, we looked at the effective yield and concluded that the spread in $y_{\rm eff}$ cannot be explained by closed box evolution. To further examine the scatter in the MZR, we calculated the variation of gas fractions in the mass-metallicity relation, by comparing galaxies in the scatter above and below the relation with galaxies on the relation. We find for the first time a clear relation in the variation of gas content in the mass-metallicity relation. We showed that galaxies with higher oxygen abundances have lower gas fractions, whereas galaxies with lower oxygen abundances have higher gas fractions. This is a good argument for in- and outflow of low metallicity gas. We found that inflow of gas is the most likely cause of the deviation from the closed box model. We compared our results to those of Zhang et al. (2009)

8 Discussion

Throughout this study, we use estimates for various parameters derived by using the Charlot & Longhetti model. It is important to note, that those models assume that the gas is ionized only by the most massive stars. It neglects that gas can also be ionized by hot intermediate and low-mass stars and planetary nebulae. Therefore the model may disregard additional physical processes that contribute to galaxy spectra. In section 3 we also make a number of assumptions in our determination of $\mu_{\rm gas}$, that are well supported by observations, but may not be true for *all* galaxies.

The result from our study about the minimum set of emission lines, is purely qualitative. Our sample (Sample I) is too small for statistical analysis, because the number of galaxies per bin is to small, hence the

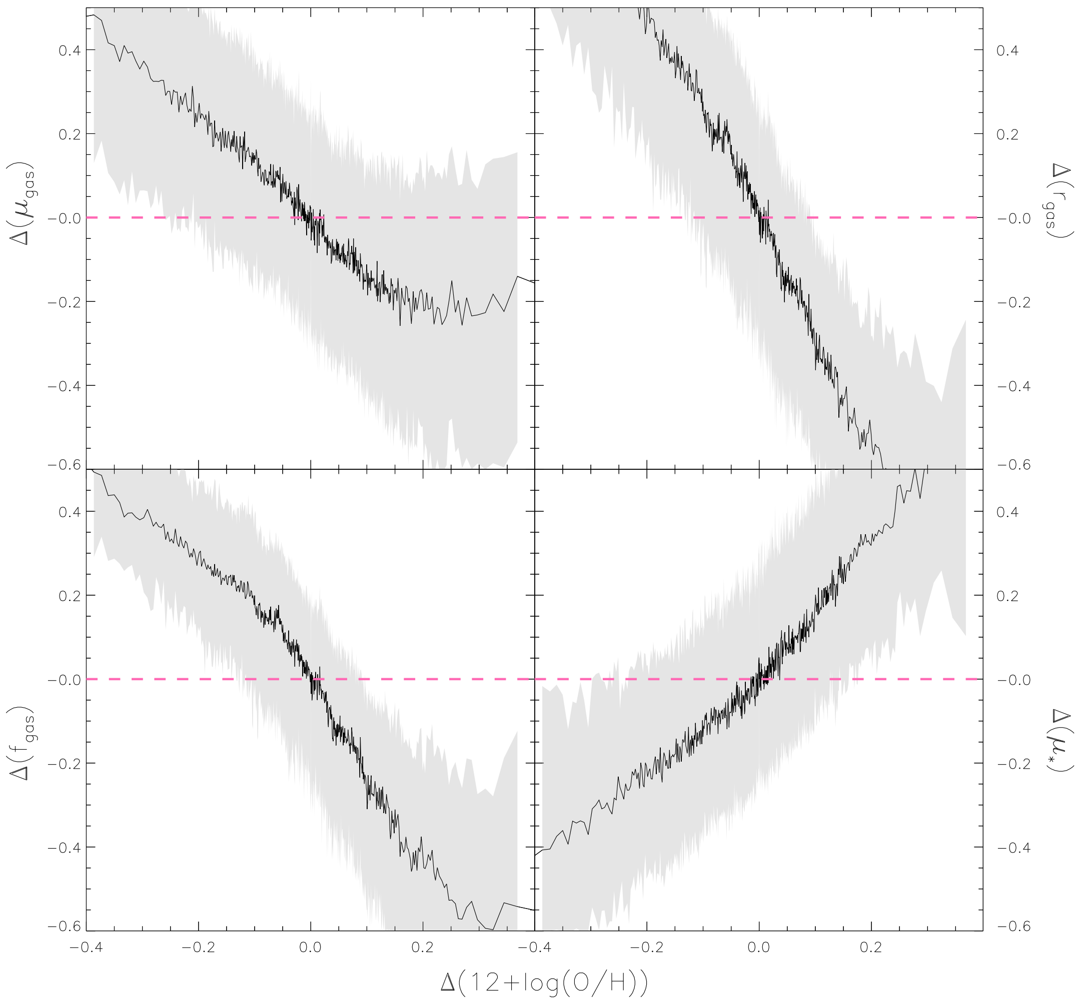

Figure 23: Variation of different parameters for Sample II. Negative values for the oxygen abundance indicate galaxies that lie below the median trend of the MZR, positive values indicate those above that. Negative values for the different parameters indicate lower values than those that lie on the relation, positive values indicate higher values. The black line demonstrates the median trend for the variation. The shaded area encloses 68% of the data. The median trends are calculated by calculating the median values of the indicated parameter in bins of $\Delta(12+\log(\mathrm{O/H}))$, each bin containing 250 objects. The 2-σ spread is calculated by computing the 0.16 and 0.84 quantile and subtracting the first from the latter. The reader will immediately spot the clear trends in the variation of μ_{gas}, r_{gas}, f_{gas} and μ_*. We see that when the gas mass fraction increases, the metallicity decreases. Typically, when you double the amount of gas in a galaxy, the metallicity decreases with a factor of 1.5. Similar trends can be seen for μ_{gas} and r_{gas} . The trends continue above the median trend of the MZR. A plausible explanation for these results is, that galaxies that lie below the median trend of the MZR, have had recent inflow of metal-poor gas. The variation in gas above the MZR, can be explained by outflow of gas. We also see, that increasing μ_* has the effect of increasing the metallicity. This is reasonable, for a higher amount of stars will eject a higher amount of heavy elements into the ISM (which is in agreement with the closed box model).

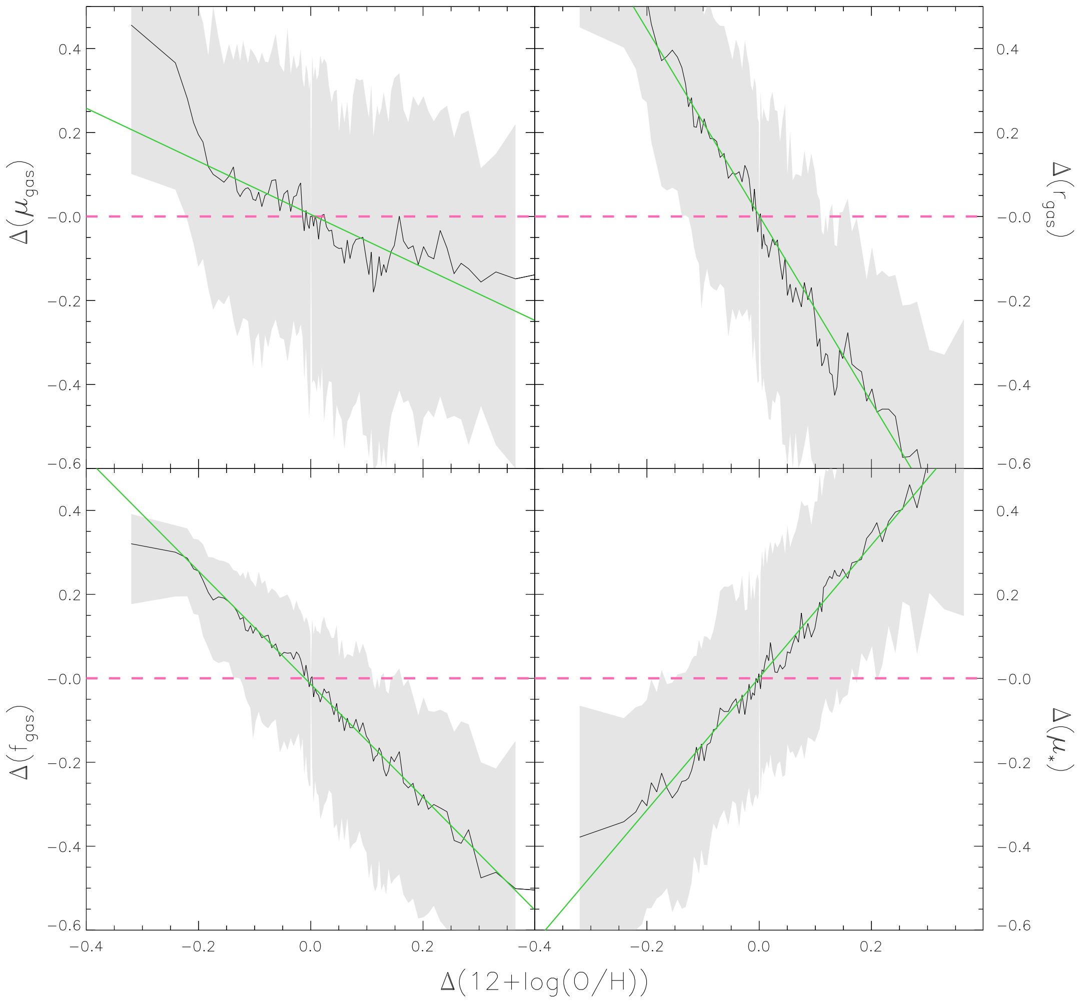

Figure 24: Variation of different parameters in the MZR for low-mass galaxies. Negative values for the oxygen abundance indicate galaxies that lie below the median trend of the MZR, positive values indicate those above that. Negative values for the different parameters indicate lower values than those that lie on the relation, positive values indicate higher values. The black line demonstrates the median trend for the variation. The shaded area encloses 68% of the data. The green line shows the linear fit through the median trend. The median trends are calculated by calculating the median values of the indicated parameter in bins of $\Delta(12 + \log(O/H))$, each bin containing 250 objects. The 2-σ spread is calculated by computing the 0.16 and 0.84 quantile and subtracting the first from the latter. The overall trends for the variation do not deviate much from the trends computed for the entire Sample II. However, the trends do differ from those derived for high-mass galaxies, as shown in figure 25. The trend in variation for $f_{\rm gas}$ and $\mu_{\rm gas}$ is steeper for high-mass galaxies, than for their low-mass counterparts, indicating that adding gas to a low-mass galaxy, has a more significant effect on the metallicity of that galaxy, than for a high-mass galaxy.

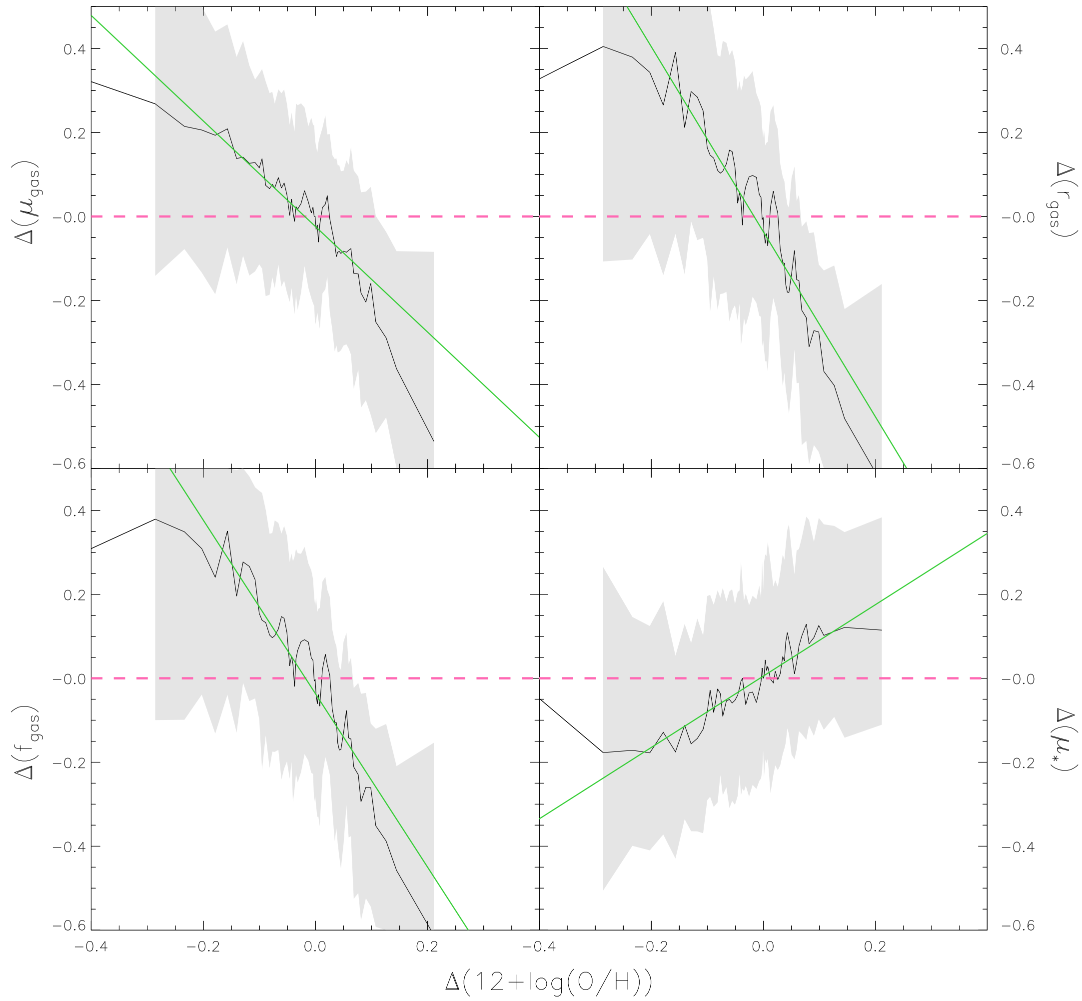

Figure 25: Variation of different parameters in the MZR for high-mass galaxies. Negative values for the oxygen abundance indicate galaxies that lie below the median trend of the MZR, positive values indicate those above that. Negative values for the different parameters indicate lower values than those that lie on the relation, positive values indicate higher values. The black line demonstrates the median trend for the variation. The shaded area encloses 68% of the data. The green line shows the linear fit through the median trend. The median trends are calculated by calculating the median values of the indicated parameter in bins of $\Delta(12 + \log(O/H))$, each bin containing 250 objects. The 2-σ spread is calculated by computing the 0.16 and 0.84 quantile and subtracting the first from the latter. The overall trends for the variation do not deviate much from the trends computed for the entire Sample II. However, the trends do differ from those derived for low-mass galaxies, as shown in figure 24. The trend in variation for $f_{\rm gas}$ and $\mu_{\rm gas}$ is steeper for high-mass galaxies, than for their low-mass counterparts, indicating that adding gas to a low-mass galaxy, has a more significant effect on the metallicity of that galaxy, than for a high-mass galaxy.

uncertainty (which goes down with the square root of the number of objects) will remain large. Therefore looking at trends and determining when they disappear is a good way to get results, although they cannot be quantified. For $\mu_{\rm gas}$, we looked at the trend between $\mu_{\rm gas}$, the Hα/Hβ ratio and the oxygen abundance. Since the Hα/Hβ ratio is a measure for dust abundance and $\mu_{\rm gas}$ is derived from the oxygen abundance and the dust, a clear trend is expected, when $\mu_{\rm gas}$ is well-estimated. However, when $\mu_{\rm gas}$ cannot be properly constrained, the physical relation is expected to disappear. This is indeed what happens in our examination. Therefore looking at this trend and determining when it disappears, will give us physically meaningful results.

We further tested the parameters of the $\mu_{\rm gas}$ equation by comparing our estimates for $\mu_{\rm gas}$ to estimates from Leroy et al. (2008) and we found a discrepancy at low Z. The discrepancy between $\mu_{\rm gas}$ from emission lines and $\mu_{\rm gas}$ from CO emission, has also been found by Meixner et al. (2009). We substituted different estimates for Z and $\tau_{\rm V}$, in order to check whether our $\mu_{\rm gas}$ estimates were accurate. We did not find an indication that our estimates were wrong. We did however not test the constant prefactor 0.2 and ξ, so this might be useful to do. It could also be, that measuring gas content from CO emission, like Leroy et al. did, is not an accurate method, as discussed in section 4.

We found that the median trend effective yield (see figure 21 can be explained by the closed box model, although it decreases at high and low mass. At $10^{9.3}M_\odot < M_{\rm tot} < 10^{10.5}M_\odot$, $y_{\rm eff}$ is even larger than the true yield, which is unexpected. This might be caused by aperture effects. We assumed that what is measured within the fibre apertures is typical for the galaxies, but since for nearby galaxies only the innermost part of the galaxy is measured, we might measure higher abundances than the true average abundance of the galaxy, causing our value of $y_{\rm eff}$ to be to high. Another effect is that the gas fractions that are derived for nearby galaxies are too low, since one will find that there are larger gas fractions towards the edges of the galaxies. The slight decrease in the median effective yield at masses higher than $10^{10.5}M_\odot$ might be due to the fact that the typical gas fractions are higher at $10^{9.3}M_\odot < M_{\rm tot} < 10^{10.5}M_\odot$, and gas fractions decrease towards higher masses.

The large scatter in the effective yield and MZR could be very well explained by in- and outflow of gas. Note that this scatter, is not the uncertainty. The uncertainty is the scatter that can be seen in the median trend, which is ≈0.05 dex, indicating that the median trend is well-defined. We found that at fixed $M_{\rm tot}$, galaxies that are below the median trend in the mass-metallicity relation have higher gas fractions than galaxies on the median trend and galaxies above the median trend have lower gas fractions. This is a strong argument, that there occurs metal-loss by inflow of low-metallicity gas. We also argue that galaxies above the median trend lost gas due to outflow. This is in agreement with what Zhang et al. (2009) found, but our findings contradict the explanation Tremonti et al. (2004) give for metal-loss. They argue that metal-loss is due to outflow, instead off inflow. They did however not find such a strong dependency between gas content variation and metallicity at fixed $M_{\rm tot}$.

Acknowledgments

First and foremost we would like to thank our supervisor Jarle Brinchmann for all his helpful suggestions, support and his wonderful IDL library. We like to thank Ignas Snellen, Demerese Salter and Kalle Torstensson for their support and useful comments during the bachelor research meetings and for their help during the presentations. We also would like to thank J. van de Sande for his help with our fitting problem. Funding for the SDSS and SDSS-II has been provided by the Alfred P. Sloan Foundation, the Participating Institutions, the National Science Foundation, the U.S. Department of Energy, the National Aeronautics and Space Administration, the Japanese Monbukagakusho, the Max Planck Society, and the Higher Education Funding Council for England. The SDSS Web Site is http://www.sdss.org/. The SDSS is managed by the Astrophysical Research Consortium for the Participating Institutions. The Participating Institutions are the American Museum of Natural History, Astrophysical Institute Potsdam, University of Basel, University of Cambridge, Case Western Reserve University, University of Chicago, Drexel University, Fermilab, the Institute for Advanced Study, the Japan Participation Group, Johns Hopkins University, the Joint Institute for Nuclear Astrophysics, the Kavli Institute for Particle Astrophysics and Cosmology, the Korean Scientist Group, the Chinese Academy of Sciences (LAMOST), Los Alamos National Laboratory, the Max-Planck-Institute for Astronomy (MPIA), the Max-Planck-Institute for Astrophysics (MPA), New Mexico State University, Ohio State University, University of Pittsburgh, University of Portsmouth, Princeton University, the United States Naval Observatory, and the University of Washington.

References

Baldwin J.A., Phillips M.M. & Terlevich R. 1981, PASP, 93, 5B

Bernard et al. 2008, AJ,

Brinchmann J. et al. 2004, MNRAS, 351, 1151

Brinchmann J., Kunth D. and Durret F. 2008, A&A, 485, 657

Brinchmann J., Pettini, M., Charlot S. 2008, MNRAS, 385, 769

Brinchmann J. et al. (in prep)
Bruzual G.A. & Charlot S. 1993, ApJ, 405, 538
Charlot S. & Fall S.M. 2000, ApJ, 598, 718
Charlot S. and Longhetti, M. 2001, MNRAS, 323, 887
Ellison S.L. et al. 2008, AJ, 135, 1877
Ferland G.J. 1996, hbic.book, F
Garnett D.R. 2002, AJ, 581, 1019
Kannappan S.J. et al. 2004, ApJL, 611, L89
Kauffmann G. et al. 2003, MNRAS, 341, 33
Kennicutt R.C., Jr. 1998, ApJ, 498, 541
Lequeux J. et al. 1979, A&A, 80, 276A
Leroy A.K. et al. 2008, AJ, 136, 2782
Meixner M. et al. 2009, Published online at http://ssc.spitzer.caltech.edu/mtgs/ismevol/
Neininger N. et al. 1998, Nature, 395, 871
Osterbrock D.E. & Ferland G.J. 2006, *Astrophysics of Gaseous Nebulae and Active Galactic Nuclei* (Sausalito, California: University Science Books)
Pagel B.E.J. 1997, *Nucleosynthesis and Chemical Evolution of Galaxies* (Cambridge: Cambridge University Press)
Pettini M. & Pagel B.E.J.2004, MNRAS, 348, L59
Shields J.C. & Kennicutt Jr. R.C. 1995, ApJ, 454, 807
Spitzer Jr.L. 1978, *Physical Processes in the ISM* (New York: Wiley)
Stasińska G. 1980, A&A, 85, 359
Strauss M.A. et al. 2002, AJ, 124, 1810
Tremonti C.A. et al. 2004, AJ, 613, 898
Walter F. et al. 2008, AJ, 136, 2563
Wild V. et al. 2007, MNRAS, 381, 543
York D.G. et al. (in prep)
Zhang W., et al. 2009, MNRAS (accepted), arXiv e-print ,arXiv:0902.2392v2